2.09 Å resolution structure of *E. coli* HigBA toxin-antitoxin complex reveals an ordered DNA-binding domain and intrinsic dynamics in antitoxin

Pankaj Vilas Jadhav[1,$], Vikrant Kumar Sinha[1,$], Saurabh Chugh[3], Chaithanya Kotyada[1, 5], Digvijay Bachhav[1,6], Ramandeep Singh[3], Ulli Rothweiler[4,*], and Mahavir Singh[1,2,*]

[1]Molecular Biophysics Unit, Indian Institute of Science, Bengaluru, 560012, INDIA

[2]NMR Research Centre, Indian Institute of Science, Bengaluru, 560012, INDIA

[3]Tuberculosis Research Laboratory, Translational Health Science and Technology Institute, Faridabad-Gurugram Expressway, Haryana 121001, INDIA

[4]The Norwegian Structural Biology Centre, Department of Chemistry, The Arctic University of Norway, N-9037 Tromsø, Norway

[5]Current address: Mazumdar Shaw Center for Translational Research, Bengaluru, 560099, INDIA

[6]Current address: Qlaar Solution Private Limited, Bengaluru, 560066, INDIA

[$] Equal contribution

* To whom correspondence should be addressed:

Email: ulli.rothweiler@uit.no (U.R.); singh@iisc.ac.in (M.S.)

Key words: X-ray structure, intrinsic dynamics, HigBA, toxin-antitoxin, MD simulation, NMR spectroscopy

Abstract

The toxin-antitoxin (TA) systems are small operon systems that are involved in important physiological processes in bacteria such as stress response and persister cell formation. E. coli HigBA complex belongs to the type II TA systems and consists of a protein toxin called HigB and a protein antitoxin called HigA. The toxin HigB is a ribosome-dependent endoribonuclease that cleaves the translating mRNAs at the ribosome A site. The antitoxin HigA directly binds the toxin HigB, rendering the HigBA complex catalytically inactive. The existing biochemical and structural studies had revealed that the HigBA complex forms a heterotetrameric assembly via dimerization of HigA antitoxin. Here, we report a high-resolution crystal structure of E. coli HigBA complex that revealed a well-ordered DNA binding domain in HigA antitoxin. Using SEC-MALS and ITC methods, we have determined the stoichiometry of complex formation between HigBA and a 33 bp DNA and report that HigBA complex as well as HigA homodimer bind to the palindromic DNA sequence with nano molar affinity. Using E. coli growth assays, we have probed the roles of key, putative active site residues in HigB. Spectroscopic methods (CD and NMR) and MD simulations study revealed intrinsic dynamic in antitoxin in HigBA complex, which may explain the large conformational changes in HigA homodimer in free and HigBA complexes observed previously. We also report a truncated, heterodimeric form of HigBA complex that revealed possible cleavage sites in HigBA complex, which can have implications for its cellular functions.

Introduction

Toxin-Antitoxin (TA) systems are pairs of genes that are either located on bacterial plasmids or integrated in the bacterial genome. One of the gene of this pair codes for a toxin, which causes growth arrest by interfering with vital cellular processes and the other gene codes for a cognate antitoxin, which neutralizes the toxin's activity during normal growth conditions [1-3]. When the bacterial cell encounters stressful conditions, often the antitoxin is selectively degraded, allowing toxin to exhibit its activity leading to growth arrest and/or dormancy [4-6]. The major biological functions of TA systems are: post-segregational killing [7], abortive infection [8], and persister cell formation [9]. The TA systems are classified into Type I to Type VI on the basis of how the antitoxin inactivates the toxin and the nature of antitoxin molecule [10, 11]. The toxins in all types of TA systems are protein molecules, however the antitoxin can be a protein or an RNA molecule [10].

Type II systems are the most prevalent and are well-studied TA systems. A typical Type II TA system consists of a toxin and an antitoxin, where both toxin and antitoxin are proteins [2, 12]. A type II antitoxin mainly has two functions, first it binds to the toxin and inhibit its activity and; second it acts as autorepressor by binding the promoter region thereby regulating the expression of the TA operon [13, 14]. The type II toxins inhibit bacterial growth by targeting essential cellular process like DNA replication [12, 15], translation [16, 17], etc. Majority of the type II toxins such as RelE, HigB, MqsR and MazF are endoribonucleases. The toxins can be ribosome dependent (examples RelE, HigB, YoeB) [16, 18, 19] or ribosome independent (examples MqsR, MazF) endoribonucleases [20, 21]. The ribosome dependent endoribonucleases share a common microbial RNase T1 like fold in their structures [22] and cleave the translating mRNAs at the A-site of the ribosomes [16, 18, 19, 22]. Some toxins display codon specific cleavage activity, for example RelE cleaves mRNA at UAG and CAG codons [16] and YafQ cleaves at AAA codon [23], while others have a broad range of specificity where they can cleave different mRNAs. Particularly, HigBA (host inhibition of growth) family of toxin provides a good example for such a case as the HigB toxin has been shown to cleave A-rich codons [19].

The HigBA is a unique ribosome dependent type II TA system. In HigBA operon, unlike most of the type II TA systems, the HigB toxin gene precedes the antitoxin HigA gene [24]. The E. coli K12 toxin HigB is homologous to RelE family of toxins [25]. Previous structural studies on E. coli K12 HigBA system had revealed that HigBA complex is a heterotetrameric structure formed by two interacting heterodimer of HigA-HigB, resembling an overall V shape configuration [26]. The toxin has an RNase T1 like fold consisting of three N-terminal α helices (α1-α3) followed by an antiparallel β-sheet (consisting of β1-β3

strands) and a C-terminal α helix (α4). On the other hand, the antitoxin HigA is a completely helical protein. HigA structure can be segmented into three parts: the N-terminal dimerization domain (helices α1 and α2), the central part (helices α3-α6) that interacts with the toxin HigB and the C-terminal DNA binding domain (DBD) (helices α7-α9). Interestingly, the binding of the antitoxin HigA to toxin HigB does not occupy or block the active site of HigB toxin, supporting the hypothesis that HigA antitoxin inhibits toxin activity by sterically hindering its binding to ribosome [19, 26].

However, there are outstanding questions that remain to be answered. For example, the role of putative active site residues in toxin HigB's function is not systematically probed. The mechanism of release of HigB toxin from HigBA tetramer is not well studied. The structure of DNA binding domain of HigA in HigBA complex is not well defined and the structural basis of DNA binding by HigA antitoxin remained unknown.

The existing structure of E.coli K-12 HigBA lacked the electron density for key residues in both toxin HigB and antitoxin HigA, due to the low resolution (2.7 Å) of the structure [26]. Here we report a 2.09 Å crystal structure of HigBA complex from E. coli K-12 revealing the electron density for the missing residues in both toxin HigB and antitoxin HigA. Especially, in the case of HigA we observed structured DNA binding domain (DBD), consisting of four helices (α6 to α9) with a compact hydrophobic interior. Using gel-mobility shift assays, SEC-MALS, and ITC methods we have probed the interaction of HigBA complex with DNA sequence from its promoter region. Based on these results, we have generated a model of HigBA – DNA complex that explains the plausible modes of promoter DNA binding by HigA antitoxin, which has implications in understanding the transcriptional regulation of HigBA operon. Using NMR and CD spectroscopy methods in conjunction with the all atom MD simulations, we observed that the antitoxin HigA is intrinsically dynamic in solution. This may help to understand the large conformational changes that HigA has been reported to undergo from free form to bound (HigBA) forms [27, 28]. Furthermore, we report a crystal structure of the truncated, heterodimeric HigBA complex that suggests the possible proteolytic cleavage sites in toxin HigB and antitoxin HigA. We have also shown that mutation of key, putative catalytic site residues in toxin HigB results in restoration of bacterial growth. Overall, these results further our understanding of HigBA TA system's assembly, activation, and regulation.

Experimental procedures

Protein expression and purification

The HigA and HigB proteins were co-expressed in E. coli BL21 Rosetta (DE3) cells transformed with pETDuet-1 plasmid in which the toxin HigB was cloned in first multiple

cloning site (MCS) with 6X Histidine purification tag at N-terminal and the antitoxin HigA was cloned in the second MCS with no purification tag. Full-length HigA was also cloned in pET28a vector for the expression of the antitoxin alone with an N-terminal 6X-Histidine tag. For the protein expression, bacterial cells were grown at 37 °C till the OD 600 nm reached 0.7, after which cells were induced for protein expression with 1 mM IPTG at 20 °C for 16 h. The cells were harvested by centrifugation at 6000 rpm for 15 min. The cell pellet was resuspended in lysis buffer (20 mM Tris, 300 mM NaCl, pH 7.5) and lysed by sonication. Cell lysates were centrifuged for 1 h at 13000 rpm and supernatant was loaded on to a 5 ml Ni^{2+}-NTA Sepharose affinity column (GE Healthcare) at 4 °C. The proteins were eluted using elution buffer (20 mM Tris, 300 mM NaCl, 250 mM imidazole, pH 7.5). The elution fractions were analyzed for protein of interest using SDS-PAGE. Fractions containing the proteins were pooled and concentrated and further purified by Ion exchange chromatography followed by purification and buffer exchange (20 mM Tris, 100 mM NaCl, pH 7.5) by size exclusion chromatography (SEC) using a Superdex 75 column (GE Healthcare). For ^{15}N labelled HigA the cells were grown in M9 minimal media containing $^{15}NH_4Cl$ as the sole source of nitrogen.

Crystallization and structure determination

HigBA complex was crystallized using hanging drop vapour diffusion method. The crystals for HigBA tetramer complex appeared within a week at a concentration of 15 mg/ml protein at 20˚C in 0.2 M KCl, 0.05 M Tris-Cl pH 7.5, 0.05 M $MgCl_2$ and 15% PEG 3350 condition. For HigBA heterodimer, crystals appear after a month at 20˚C in 0.05 M $MgCl_2$, 0.1 M Tris, pH 7.5, 0.2 M KCl and 8-20% PEG3350. The X-ray diffraction data sets were collected at Berlin synchrotron source, (BESSY). The crystals diffracted to 2.09 Å and 2.3 Å resolutions for HigBA tetramer and HigBA heterodimer, respectively. The diffraction data sets were processed by iMosflm and XDSAPP software [29-31]. The structures were solved by Molecular Replacement method using the reported 2.7 Å resolution structure of HigBA complex (PDB 5IFG) as the search model. Coot [32] and Phenix [33] were used for iterative model building and refinement. The final model of HigBA heterotetramer has final R_{work}/R_{free} of 0.195 and 0.236 whereas HigBA heterodimer has final R_{work}/R_{free} of 0.2604 and 0.2975. The model quality was determined using MolProbity [34] of the PHENIX validation suite.

NMR spectroscopy

2D ^{1}H-^{15}N TROSY HSQC NMR spectrum of HigA antitoxin was recorded on Bruker 700 MHz, equipped with a cryoprobe at 298K. 550 µL samples of 200 µM concentration were prepared in 20 mM Sodium phosphate, 100 mM NaCl, 5 mM DTT, pH 7.5 with 10% D_2O added for spectrometer deuterium lock.

Protein-DNA gel shift assay

33 bp long ds Pal-1 and Pal-2 DNAs were generated by annealing two complementary oligonucleotide strands (Sigma-Aldrich). Reaction mixtures of 10 µL volume containing DNA and HigBA complex in different ratios, where the DNA concentration was constant (10 µM) while the protein concentration was varied, were assembled in lysis buffer (20 mM Tris, 300 mM NaCl, pH 7.5) and incubated for 2 h in ice. The samples were electrophoresed on a native 8% polyacrylamide gel with 0.5XTBE (Tris-borate with EDTA) visualized by toluidine blue DNA staining.

SEC-MALS

SEC-MALS was performed to determine the molecular weight of HigBA and DNA bound HigBA complex in solution. Shimadzu chromatography system equipped with a miniDAWN TREOS MALS detector and a WATERS 2414 refractive index (RI) detector was used for the experiment. The system was calibrated using bovine serum albumin (BSA). 100 µL of purified, centrifuged and degassed samples were used for the experiment. Biorad Enrich S70 (10/300) column was used for protein complex whereas GE S200 (10/300) column was used for the protein-DNA complex. The molecular weight was calculated using ASTRA VI software (Wyatt Technology).

Isothermal Titration Calorimetry (ITC)

ITC experiments were performed using a VP-ITC machine (MicroCal, USA) at 30 °C. The proteins (HigBA tetramer and HigA homodimer) and DNA (Pal-1 DNA) samples were prepared in buffer containing 20 mM Tris, 150 mM NaCl, pH 7.5 and thoroughly degassed before experiments. For the titrations, the sample cell was filled with 10 µM of the DNA, which was titrated against 200-300 µM of HigBA and HigA samples from the syringe. Separate protein into buffer run were performed as control to know the heat of dilution of protein into the buffer. Thirty injections of the titrant were performed at an interval of 180 s. The heat of dilution of ligands in buffer were subtracted from the integrated heat data and the data was fit for one site-binding model. The analysis was done using ORIGIN-5 software provided by the vendor. All the parameters were kept floating during the data fitting.

CD spectroscopy

CD spectra of HigA were recorded on a JASCO J-715 spectropolarimeter. The experiments were performed in 1 cm path length cuvette (Hellma Analytics) at 25°C at a scanning speed of 100 nm/min with a response time of 4 s. The wavelength scan was done from 190 nm to 260 nm. 7 µM of the HigA protein sample was used for the experiment. The average of three spectral scans was taken for each sample followed by baseline correction to negate the contribution from the buffer. For the thermal melting experiment, the changes in the secondary structure of HigA were observed by recording the CD signal at 208 nm as a

function of temperature. The temperature of the sample was changed at a rate of ~1 °C/min from 15 °C to 90 °C. The melting temperature (Tm) was obtained by fitting the experimental data points (CD signal versus temperature) with a sigmoidal function for two sate transition.

E. coli growth assays

For growth inhibition assay, wild type copy of HigB was PCR amplified using pET-Duet HigBA as template DNA. The PCR product was verified by sequencing and cloned using Nde I/Hind III restriction enzymes in pET28b vector. Mutants HigB constructs (HigB-Δα4, HigB-D49A/N50A, and HigB-R68A) were generated using site directed mutagenesis of wild-type HigB construct in pET28b expression vector. These plasmid constructs were transformed in BL-21 (λ DE3, pLysS) and transformants were selected on LB agar plates supplemented with kanamycin and chloramphenicol. For protein expression, cultures were grown till OD600 nm of ~0.8 and induced with the addition of 1mM IPTG. For spotting assay, at time zero and 5 h post-induction, 10-fold serial dilutions were prepared and spotted on LB agar plates.

Molecular Dynamic Simulation

The crystal structure of HigBA complex (PDB 6KML) was used for all atoms molecular dynamics (MD) simulation using GROMACS (GROningen MAchine for Chemical Simulations) 5.1 package [35]. PDB structure of HigBA complex was processed to GROMACS file format using PDB2gmx module and GROMOS96 force field [36] was used during this process. Cubic box was generated using editconf module where HigBA complex was placed at the center of the box and distance of all edges of the box were 1.0 nm from the complex. This cubic simulation box of HigBA complex was solvated with SPC/E water model. Further, this solvated system of charged HigBA complex was neutralized by adding chloride and sodium ions as counter ions. This solvated electro neutral system was minimized energetically using steepest descent minimization algorithm followed by conjugate gradient algorithm. Both algorithms included maximum 50,000 minimization steps and maximum force below 1000 kJ $mol^{-1}nm^{-1}$. Energetically minimized system was equilibrated for 100 ps duration at temperature 300 K first with NVT ensemble (constant Number of particles, Volume, and Temperature) and subsequently with NPT ensemble (constant number of particles, pressure, and temperature). In both NVT and NPT ensembles, Berendsen thermostat was included in temperature coupling with time constant at 0.1 ps and constraint_algorithm LINCS [37] was included in bond parameter. In NPT, additional Parrinello-Rahman barostat was included in pressure coupling at 1 bar. This equilibrated system contained all requirements to perform MD simulation for 100 ns. MD simulation generated large trajectories were further analyzed for the root means square deviation (RMSD) generated using the g_rms module and RMSD graphs were plotted using GRACE tool (https://plasma-gate.weizmann.ac.il/Grace/).

HigA crystal structure (PDB 6QJ4) was obtained from RCSB Protein Data Bank [38]. Using symmetry of HigA crystal structure HigA homodimer structure was generated and subjected to MD simulation with similar protocol mentioned for HigBA complex.

Principal component analysis and preparation of free energy landscape

In order to examine significant combined motions in the MD simulation trajectory of HigBA complex, covariance matrix dependent principal component analysis (PCA) was performed [39, 40]. Atomic fluctuations in MD simulation trajectory of HigBA complex were used to generate covariance matrix and subsequently it was diagonalized. The 'g_covar' and 'g_anaeig' utilities were used for construction of covariance matrix and analysis respectively. Initial ten projection eigen vectors from MD simulation trajectory of HigBA complex were generated followed by cosine content dependent analysis. 'g_analyze' utility included in GROMACS was used for the calculation of cosine contents of all generated projection eigenvectors. Here, cosine content values of the two projection eigenvectors from diagonalized covariance matrix was calculated to be below 0.2. Usually, low value cosine contents containing projection eigenvectors, which corresponds to principal component 1 (PC1) and principal component 2 (PC2) contain essential elements to generate the free energy landscape (FEL) [41]. FEL maps (2D and 3D) were generated using Mathematica 9 (Wolfram Research, Inc., Mathematica, Version 9.0) showed free energy based different conformational ensembles of proteins, including the possible native conformation (local minima). Local minima structures of the FEL basin were generated in PDB file format and further analyzed using visualization tool UCSF Chimera [42].

Model building of HigBA – DNA complex

To generate HigBA-DNA model, we used the crystal structure of HigBA complex determined in this study (PDB 6KML). 33 bp Pal-1 DNA sequence (5' ATTCATCCGTTGCCAATCTGGCAACGGATGTTA 3') was used to generate double stranded DNA (dsDNA) using 3D-DART online server [43]. We used two HigBA complexes and one dsDNA to build HigBA-DNA model using UCSF Chimera visualization software [42] Furthermore this HigBA-DNA model was subjected to energy minimization using AMBER99SB force field [44] in GROMACS 5.1 package [45].

Results and Discussion

2.09Å resolution crystal structure of HigBA complex revealed a well-ordered DNA binding domain in antitoxin HigA

E. coli K-12 HigB and HigA were cloned in pETDuet-1 vector and co-expressed as HigBA complex in E. coli BL21 Rosetta (DE3) cells. The complex was purified initially using Ni-NTA

affinity chromatography, followed by size exclusion chromatography (SEC). The SEC profile showed that the complex eluted as a tetramer of HigBA complex with combined molecular weight of ~ 54 kDa. A 2.7 Å resolution structure of HigBA complex had previously been determined [26]. This structure had revealed the overall architecture of E. coli HigBA complex and the molecular basis of antitoxin HigA binding to toxin HigB. However, the electron densities for several key residues/regions were missing in the structure likely due to the lower resolution. For example, residues 101 to 104 were missing in toxin HigB structure. Similarly, in antitoxin HigA regions containing residues 95 to 104 and 131 to 138 in the C-terminus that constitute the DBD, were missing [26]. Very recently, a 3.1 Å resolution structure of homologous Shigella flexneri HigBA complex was reported (PDB 5YCL) [28]. Though the structure is similar to the E. coli HigBA complex, in this structure too, the DBD of HigA had missing residues/regions [28].

Here we report crystallization of E. coli HigBA complex under different set of crystallization conditions. Under new conditions, the HigBA complex crystallized in $P2_1$ space group and diffracted to a higher resolution of 2.09 Å at a synchrotron X-ray source (Table 1). The structure of the complex was solved by the molecular replacement method using PDB 5IFG [26] as the search model. The structure was refined to a final R_{work} of 19.5% and an R_{free} of 23.6%. Table 1 summarizes the final data collection and refinement statistics. The overall architecture of the structure is similar to previously reported structures however with some significant improvement (Figure 1A-C and Supplementary Figure S1A-C).

The HigBA complex is a heterotetramer formed by interaction of two dimers of HigA-HigB, forming a V shaped structure. The two dimers are structurally symmetric and almost identical (all Cα rmsd of 0.467) therefore the structure has an internal two-fold symmetry. In the HigBA tetramer structure, only the antitoxin HigA protomers interact via an N-terminal dimerization helix and there is no interaction between toxin HigB protomers (Figure 1A). The toxin HigB consists of a α/β/α type microbial RNAse T1 fold, comprising of three N-terminal helices (α1 and α2), an antiparallel β-sheet (consisting of β1-3 strands) followed by a C-terminal α-helix (α4). The antitoxin HigA is an all helical structure consisting of three regions: the N-terminal dimerization domain (helix α1 and α2), the middle toxin-binding region (helices α3-α6), and the C-terminal, helix-turn-helix (HTH) containing DNA binding domain (DBD) comprising of helices α6 to α9. While, the existing structures [26, 28] had elegantly explained the dimerization and HigB binding by HigA, the DNA binding domain in HigA had regions missing the electron density limiting our understanding of the complete HigBA complex structure important for understanding the DNA binding by HigBA complex and antitoxin HigA.

In our current 2.09 Å resolution crystal structure of E. coli K-12 HigBA complex, the electron density for all residues (except last three residues in HigB) is present. The overall geometry of the current structure and the conformation of side chains of several residues are defined with better precision (Supplementary Figure S1A,B). While the toxin HigB and the dimerization and toxin binding domains of antitoxin HigA are similar to existing structures, the C-terminal DBD of HigA is completely defined in the new structure of E. coli K-12 HigBA complex (Figure 1B,C).

The antitoxin DBD consists of three regular alpha helices α6 to α8, which are connected via loops (L1 and L2) followed by a short left-handed π helix at the C-terminus (named α9) (Figure 2A). Helix α6 spans residues Gly79 to Tyr91, helix α7 spans residues Lys104 to Leu111, α8 spans residues Leu119 to Phe129, and short helix α9 spans residues Pro133 to Phe136. Two loops L1 and L2 connect helices α6 to α7 and α7 to α8 respectively. The DBD is a well-folded structure with a compact hydrophobic core. Sidechains of the hydrophobic residues from the helices α6 to α9 form the compact hydrophobic interior of the DBD. These include residues Ile81, Ile84, Leu87, Met88 from α6; residues Val107, Val110, and Leu111 from α7; residues Leu125, and Phe129 from α8; and residue Phe136 from α9. Both loops L1 and L2 are well ordered in the structure. Side chains of Leu98 and Ile101 from loop L1 and Leu117 from loop L2 face the interior contributing towards the hydrophobic core of the DBD. The Tyr91 from helix α6 and Phe129 from helixα8 have a stacking interaction, further cementing the hydrophobic interior (Figure 2A).

The HigA DBD interacts with the toxin HigB using the amphipathic helix α6. Side chains of polar residues Arg85, Asp89, and Gln90 from helix α6 are involved in hydrogen bonds and ionic interactions with the polar residues from the helices α2 and α3 of HigB toxin. Overall, the HigBA DBD is structurally homologues to the classical DBD present in phage 434 repressor and other proteins (Figure 2B).

HigBA heterotetramer and HigA homodimer interact with its promoter DNA with high affinity

The antitoxin HigA alone or as HigBA complex, has been shown to bind to the DNA sequences in the HigBA gene promoter region [26]. Two imperfect palindromic sequences had been identified in the promoter region namely, Pal-1 and Pal-2 (Supplementary Figure S2A) [26]. Using gel-mobility shift assays, the HigBA complex was shown to bind to both Pal-1 and Pal-2 sequences [26], however a quantitative estimation of protein-DNA complex formation was not determined. The DNA binding was attributed to the C-terminal DBD as the deletion of the DBD was shown to abolish the binding of HigBA to the DNA [26].

We initially tested binding of HigBA complex to both 33 bp Pal-1 and 33 bp Pal-2 sequences for DNA binding using gel-shift assays. Similar to the previous observations, we found that HigBA complex binds both Pal-1 and Pal-2 sequences with Pal-1 sequence giving a clean one-band shift at 1:2 DNA to protein ratio suggesting that two HigBA complexes bind to Pal-1 DNA (Supplementary Figure S2B,C). To understand the HigBA – DNA interactions in detail, we used Pal-1 DNA in further experiments. This stoichiometry was further confirmed using SEC-MALS (size exclusion chromatography, multi-angle light scattering) experiment. We analyzed both, free HigBA complex and HigBA – Pal-1 DNA complexes on SEC-MALS. The SEC-MALS analysis revealed a molecular weight of ~ 51 kDa for the free HigBA complex, which is in agreement with the expected molecular weight of HigBA heterotetramer (54.2 kDa) (Figure 3A). The SEC-MALS analysis revealed a molecular weight of ~ 116 kDa for the HigBA – Pal-1 DNA complex, which corresponds to the expected molecular weight of HigBA – Pal-1 DNA complex (122.42 kDa) in a protein to DNA stoichiometry of 2 (Figure 3A).

To quantitate and understand the energetics of protein – DNA interactions, we used isothermal titration calorimetry (ITC) experiments in next experiments. ITC experiment measures heat generated or absorbed upon binding and provides values of the equilibrium dissociation constant (K_D), the stoichiometry (n) and the change of enthalpy (ΔH). The K_D value obtained permits calculation of the change in free energy (ΔG), which together with the ΔH allows the calculation of the entropic change term, TΔS. At 30°C and under 150 mM NaCl, the antitoxin HigA homodimer showed an enthalpically driven (ΔH = -5.38±0.04 kcal/mol and TΔS = 4.94±0.92 kcal/mol) binding with Pal-1 DNA with a K_D of ~36 nM and a protein:DNA stoichiometry of ~2 (Figure 3B and Table 2). Under same condition, interestingly binding of HigBA heteroteramer to Pal-1 DNA showed different ITC isotherm. We observed that binding of HigBA with Pal-1 DNA proceeds with a positive heat change that reaches maximum at the third injection (please note that the first inject was incomplete and not used during data integration). The positive heat change then gradually decreases at subsequent injections. This hints at two sequential binding events (Figure 3C) [46]. However, we achieved best fitting of integrated data for a one site binding model. Analyzed data showed that HigBA tetramer binds to Pal-1 DNA in an entropically driven manner (ΔH = 3.96±0.08 kcal/mol and TΔS = 13.73±3.97 kcal/mol) with a K_D of ~91 nM and a protein to DNA stoichiometry of ~2, which is in agreement with results obtained from EMSA and SEC-MALS experiments (Figure 3C and Table 2). Control ITC runs of HigBA and HigA titrations into buffer that show the contributions from the heat of dilution of proteins is shown in Supplementary Figure S3A,B.

Under the reported experimental conditions, HigA homodimer binds to Pal-1 DNA with approximately 3-fold lower K_D (better binding) than HigBA heterotetramer binding to Pal-1

DNA. This suggests that HigB toxin does not significantly influences the DNA binding activity of HigA antitoxin. The binding of HigBA heterotetramer to Pal-1 DNA is an endothermic and entropically driven reaction, while the binding of HigA homodimer is exothermic reaction with favorable enthalpic and entropic contributions (Figure 3B,C and Table 2). Generally, unfavorable enthalpy change is attributed to the loss of favorable contacts of protein and DNA with solvent molecules (water and ions) [47]. This release of ordered and bound solvent molecules from DNA and proteins results in favorable entropic change that drives the binding. In the two ITC experiments reported here, the DBDs in HigA protomers and the DNA are identical, however the dynamics of HigBA complex vs. HigA dimer as well as the conformational change in DNA in HigA – DNA vs. HigBA – DNA complexes may be different. Therefore, the loss of water molecules from polar surfaces and redistribution of salt ions would be different in HigA – DNA vs. HigBA – DNA complexes, resulting in distinct thermodynamic signature.

Plausible model of HigBA-DNA complex

We generated a model of Pal-1 DNA – HigBA tetramer complex using an integrative modeling approach based on the observations detailed in the previous section (please see details in Experimental Procedures). Structurally homologous DBDs in other proteins have shown that the dimer of DBD binds to the major grove of operator DNA sequences [48-50]. In particular, DBD of Proteus vulgaris and phage 434 repressor, which are structural homologs of DBD of HigA (Figure 2B) bind in dimer form by placing third α-helix in major groove of DNA (PDBs 6CHV and 2OR1) [48, 49]. Recently it was postulated that the helix α7 of HigA DBD likely constitute the DNA major groove binding helix and along with helix α8 constitute the helix-turn-helix (HTH) of DBD [27, 28]. The helices α7 and α8 of E. coli HigA DBD structurally align with the third and fourth helices of Proteus vulgaris HigA and phage 434 repressor DBDs (Figure 2B). Based on these collective observations, we present a model where two protomers of HigA in HigBA tetramer bind to 33 bp Pal-1 DNA with helix α7 binding the major groove of DNA to generate specific HigA – DNA complex (Figure 3D). Considering the symmetry of DNA sequences (palindromic nature), the helix α7 is inserted in the CG bp centered major groove of the Pal-1 DNA sequence and helix α8 is closer to this major groove. The Pal-1 DNA sequence consists of three non-palindromic base pairs in the middle separating two reverse-complementary sequences (Figure 3D). This model explains the stoichiometry of HigBA – DNA complex observed using EMSA, SEC-MALS, and ITC experiments presented earlier (Figure 3A-C and Supplementary Figure S2B,C). Therefore, we propose that two HigBA heterotetramers bind to a 33 bp Pal-1 DNA with four DBDs in HigA protomers binding the DNA over the two palindromic repeat sequences (Figure 3D).

This proposed model shows a possible mode of promoter DNA binding by HigBA complex with implications in understanding the autoregulation of HigBA operon.

Structure of dimeric HigBA complex suggests possible cleavage sites in HigA and HigB

While screening the HigBA complex for crystallization under different conditions, HigBA crystallized in a dimeric form in one of the conditions. The structure of the hetero dimeric HigBA was solved using molecular replacement method and refined to a resolution of 2.3 Å (Figure 4A and Table 1). The HigBA heterodimer structure consists of truncated one HigB and one HigA molecule. In this structure, antitoxin HigA is devoid of helices α1 and α2 at N-terminus (the dimerization domain in tetrameric HigBA complex) and toxin HigB is devoid of C-terminal helix α4 (Figure 4B,C). Absence of dimerization domain in antitoxin HigA results in assembly of only dimeric HigBA complex.

A comparison of arrangement of molecules in the crystal packing of HigBA heterodimer and HigBA heterotetramer, clearly showed that the crystal packing in heterodimer would not allow space for the missing regions (Supplementary Figure S4A). Furthermore, we also observed that when stored for a prolonged time (>2 weeks) at 4°C, full-length HigA showed degradations as observed on a SDS-PAGE, suggesting the possibilities of full-length HigA undergoing degradation as seen in HigBA heterodimer structure (Supplementary Figure S4B).

As mentioned earlier, the HigB toxin binds to the A site of the ribosome and cleave the translating mRNA [16, 19, 21, 22]. The C-terminal region generally, in these toxins including the last helix (α4 in HigB) is important for docking of toxin to the ribosome (Supplementary Figure S5A-C) [51]. The ‘active site’ in HigB RNase toxin is away from the antitoxin (HigA) binding interface therefore, antitoxin binding does not explain the inhibition of the RNase activity of toxin HigB directly. Instead, binding of HigA to HigB results in a formation of a large HigBA heterotetrameric complex, which physically cannot access the A site in the ribosome and thereby it is rendered inactive [26]. Therefore, we postulate that the removal of helix α4 will result in reduced affinity of truncated HigB (HigB-Δα4) for the ribosome binding and have impaired RNase activity. In bacteria, TA complexes are activated during certain stress conditions such as exposure to antibiotic [52]. Generally, the intrinsically disordered antitoxin is cleaved by the cellular proteases that are expressed during stress, resulting in the release of toxin in the cell. The antitoxin HigA, however is not disordered and rather it is a well folded (all helical) protein. Therefore, how HigBA systems are activated in the cell, remains unknown. The dimer structure of HigBA presented here may suggest possible cleavage point

(removal of dimerization domain) in HigA antitoxin that may ultimately assist in toxin HigB release.

Taken together, the truncated heterodimeric HigBA structure suggests the labile regions in antitoxin HigA and toxin HigB that may have roles in activation or deactivation of HigB activity inside bacteria.

Overexpression of HigB toxin induces bacteriostasis in E. coli

As explained earlier, E. coli HigB toxin is structurally similar to the RelE family of toxins. However, the conservation of these sequences is poor, even at the catalytic centre, which makes it difficult to identify the catalytic residues based on sequence alignment. We have compared the structure HigB from E. coli HigBA complex with the ribosome bound RelE (PDB 4V7J & 4V7K) from E.coli [51] and HigB from P.vulgaris (PDB 4YZV & 4YPB) [53] (SI Figure S3). From this comparison, we identified D49, N50, K52, R68, H88 and Y91 as plausible active site residues in E. coli HigB (Figure 5A). A few of these residues were chosen for further validation of their function using site-directed mutagenesis. A single alanine mutant of R68 (HigB-R68A) and a double mutant of D49 and N50 (HigB-D49A/N50A) were generated using site-directed mutagenesis. To ascertain the role of C-terminal helix α4 in HigB, which was found missing in truncated HigBA dimer structure, we made a deletion mutant of HigB where helix α4 (residues 91-101) was deleted (HigB-Δα4). One of the putative catalytic site residues, H88 is close to helix α4, while residue Y91 is a part of the helix α4 in toxin HigB (Figure 5A).

We used bacterial growth assay to access the role of these mutant and WT HigB in E. coli. For the growth assays, pET-28b plasmids harboring either a wild type or mutants of HigB were individually transformed in BL21 (λDE3, pLysS) cells. The expression of proteins in recombinant strains was induced by the addition of 1 mM isopropyl β-D-1-thiogalactopyranoside (IPTG). The effect of overexpression of recombinant proteins on growth of E. coli in recombinant strains was quantified by measuring absorbance (at 600 nm wavelength) at regular intervals. Growth assays were also performed on solid media by spotting 10-fold serial dilutions of culture on LB agar plates (Figure 5B-D). As shown in Figure 5B, we observed that ectopic expression of wild type HigB results in severe growth inhibition in liquid cultures in comparison to strains harboring vector control. As expected, overexpression of HigB mutant proteins, HigB-D49A/N50A, HigB-R68A and HigB-Δα4 did not result in growth inhibition of E. coli (Figure 5B). In concordance with liquid culture growth inhibition assays, we observed that in comparison to parental strain, overexpression of wild type HigB protein resulted in >10,000-fold reduction in growth on solid medium (Figure 5C). We also observed that the growth patterns obtained in strains overexpressing mutant

proteins after 5 h of induction was comparable to strain harboring vector only (Figure 5C). As expected, no differences in growth patterns were observed in strains harboring parental, wild type or mutant proteins before IPTG induction (Figure 5D). Therefore, the growth assays indicate that residues D49, N50 and R68 are crucial for catalytic activity. Also, the deletion of the C-terminal helix α4 affects protein's catalytic activity, showing the importance of α4 for the catalytic activity of HigB.

Molecular dynamics simulations study reveals dynamic nature of HigA antitoxin

We performed an all atom molecular dynamics (MD) simulation of HigBA tetramer for a duration of 100 ns using GROMACS software package [35] to understand the dynamics of the HigBA complex. Root mean square deviation (RMSD) provided the initial observation of backbone atomic motion within MD trajectory of HigBA complex. From this overall MD trajectory of HigBA complex, the individual backbone RMSD plots for HigB and HigA protomers were estimated (Figure 6A). The backbone RMSD for HigBA complex ranges from a minimum value of 0.4 nm to a maximum value of 1.0 nm, during the period of 100 ns of MD simulation, which suggests high atomic transition within the trajectory. The RMSD of the HigA dimer (extracted from HigBA complex trajectory) was found similar to HigBA tetrameric complex throughout the 100 ns simulation whereas, the RMSD of HigB (~0.15 nm) was found well stable throughout the simulation period (Figure 6A). Therefore, these results suggest that the dynamics observed in HigBA complex is mainly due to the antitoxin HigA homodimer in the complex.

To explore the different conformations of HigBA tetrameric complex within the MD simulation trajectory, principal component analysis (PCA) based free energy landscape (FEL) was analyzed [39, 40]. The PCA process included the construction of covariance matrix and its diagonalization followed by projection on the eigenvector, which led to the selection of low value cosine content containing principal components (PCs). These PCs contained centered data, which provides collective correlated motion of atoms in HigBA complex simulated trajectory that hold all necessary components of the system. Among the ten generated eigenvectors, projections on two eigenvectors were observed with relevant correlation and cosine content of these two eigenvector projections (PC1 and PC2) were analyzed to a reasonable value of below 0.2. These two PCs comprised sufficient trajectory information of HigBA complex to perform FEL to generate final two-dimensional (2D) and three-dimensional (3D) FEL maps (Figure 6B,C). The 3D FEL contour map clearly illustrated a broad basin, which suggested multiple minimum energy HigBA complex ensembles (Figure 6C). This likely suggested the structural transitions in HigBA complex among the discrete conformational states with low energy barrier during simulation period of 100 ns.

Three representative minimum energy structures of HigBA complex from basin of FEL contour map were extracted for further analysis (represented by red, green, and blue triangles in Figure 6B). These three FEL representative structures were extracted from 100 ns MD simulation trajectory at 35 ns (in red), 71 ns (in green) and 90 ns (in blue). From each FEL representative structure, HigA homodimer and HigB were separated, overlaid and aligned with respect to the starting structure (in steel) (Figure 6D,E). In case of toxin HigB, the three FEL representative structures retained conformations similar to the starting structure, showing that HigB toxin maintains a stable structure during the course of simulation (Figure 6D). However, in case of antitoxin HigA, major differences in the conformations of the three FEL representative structures, with respect to starting structure, were observed (Figure 6E). While the N-terminal dimerization domain (helices α1 and α2) and the toxin binding middle region (helices α3-α5) did not show any significant change, large conformational changes were observed in the relative orientations of the C-terminal DBD (helices α6-α9) (Figure 6E). Overall, the MD simulation results presented here showed that the antitoxin exhibits; a) ns intrinsic dynamic compared to the toxin HigB; and b) large domain movement of two DBDs of HigA protomers in the HigBA complex.

We also performed an all atom molecular dynamics (MD) simulation of HigA homodimer structure (PDB 6JQ4) (Supplementary Figure S6A) for duration of 100 ns using GROMACS software package. RMSD analysis of 100 ns MD simulation trajectories showed major deviations in HigA homodimer after initial 15 ns that collapsed into a stabilized state for the remaining period of simulation (Supplementary Figure S6B). Essentially, the DBD swung and folded onto the toxin-binding region beyond 15 ns time of simulation (Supplementary Figure S6C-E). While, this shows that the DBD containing part of HigA homodimer can undergo large domain movement, it prevented us from any further analysis of the MD data.

Antitoxin HigA forms an ordered structure but it is dynamic in solution

Generally, the antitoxins across different type II TA systems contain intrinsically disordered regions. The toxin binding domains in several antitoxins are intrinsically disordered, which become ordered upon binding to the toxin. It has been hypothesized that under stress conditions, several proteases (e.g. Lon proteases) are expressed in bacterial cell that proteolytically cleave susceptible antitoxins, thereby releasing and activating the toxin [54]. Interestingly, in a recent study, TA transcript levels were shown to increase substantially in response to diverse stress conditions without liberating the toxin from the TA complex [55]. In case of HigBA system, the antitoxin has a well folded, all helical structure [38]. However, the MD simulation results presented in current study suggested intrinsic dynamic as well as large conformational sampling of HigA protomers in HigBA complex. These contrasting

observations prompted us to characterize the full length homodimeric HigA in solution using NMR and other biophysical methods.

The full-length antitoxin HigA was over-expressed and purified. The antitoxin HigA protein expectedly purified as a homodimer. The CD spectra of the HigA homodimer gave a spectra characteristic of a helical protein (Figure 7A). Thermal melting of HigA homodimer was followed using CD spectroscopy. This revealed that protein has an average melting temperature of ~ 57 °C, suggesting a stable structure (Figure 7B). We made a uniformly ^{15}N labeled HigA homodimeric protein and recorded a 2D ^{15}N-^{1}H TROSY HSQC NMR spectra of the protein. The spectra revealed good chemical shift dispersion suggesting that protein is folded in solution. However broad and non-uniform intensities of cross peaks in the spectra strongly suggested that HigA structure likely has enhanced dynamics and undergoes a conformational exchange (Figure 7C). The CD spectra, although influenced by the tertiary structure, mainly reports the secondary structural elements in the protein, whereas NMR chemical shifts are very sensitive to the tertiary structure of the protein.

Taken together, these results augment the observations of MD simulation suggesting the dynamic nature of antitoxin. As mentioned earlier, a crystal structure of full-length HigA homodimer was recently reported [38]. However, it is well established that several proteins that do not give a well-dispersed 2D ^{15}N-^{1}H HSQC spectra could still crystallize readily. Conversely, several proteins with well-dispersed 2D ^{15}N-^{1}H HSQC spectra still cannot be crystallized [56, 57]. Additives in crystallization buffer can aid in the process of crystallization. We therefore argue that although the HigA homodimer forms an ordered structure (as observed in crystal structure), it maintains the intrinsic flexibility, which is likely the reason behind the poor NMR spectral quality of the protein.

Comparison of different HigBA and HigA structures supports dynamic nature of HigA

To understand the conformational changes in the antitoxin HigA observed in different structures of E. coli HigBA complex with respect to the free HigA homodimer structure, we aligned and overlaid different reported HigA structures (Figure 8). This include, HigBA tetramer structure reported here (PDB 6KML), HigBA tetramer structure solved by Jingsi Yang et al. (PDB 5IFG) [26], and free HigA dimer structure solved by Bing-Shuang Xu et al. (PDB 6JQ4) [27]. We measured the distances between Cα atoms of selected residues in two protomers of HigA at three different locations. This includes Glu66 in the α4, Gln75 located between α5 and α6, and Arg115 in loop L1 in DBD (Figure 8). This comparison revealed a large conformational change in the antitoxin HigA homodimer. We observed that the N-terminal half (helices α1-α4) of the three structures align well with each other, however large conformational changes were observed in the C-terminal DBD harbouring, region of the

protein (Figure 8). The DBDs in two protomers of antitoxin dimer are swung ‘open’ (R115-R115’ Cα distance ~ 50.2 Å) in free form (PDB 6JQ4). However, in the HigBA complexes, the antitoxin HigA DBDs are in ‘closed’ conformation to different extent (R115-R115’ Cα distances ~ 18.2 Å and 28.1 Å in PDB 5IFG and 6KML structures respectively) (Figure 8). This is in agreement with the MD simulation based FEL analysis (Figure 6B, C, and E) and experimental observations on solution behaviour of HigA probed using CD and NMR spectroscopy methods (Figure 7). This dynamic behaviour of HigA homodimer will likely have a role in release of toxin HigB from HigBA complex and promoter DNA binding in bacteria.

Concluding Remarks

Structures of several type II toxin-antitoxin complexes of different classes have been determined in a number of studies [58]. These structures helped in understanding the assembly, activation, and regulations of these important cellular machines, which have implications in understanding the important processes such as persister cell formation and antibiotic tolerance by bacteria [59]. HigBA is a unique type II TA system in which the toxin HigB is a ribosome dependent RNase that cleave translating mRNAs. However, the mechanism of activation of E. coli HigBA as well as the autoregulation of HigBA operon is not well understood.

A previously determined structure of E. coli HigBA TA complex had elegantly revealed the overall organization and mechanism of antitoxin HigA binding to toxin HigB [26]. This structure lacked the electron density of key residues in both toxin HigB and antitoxin HigA. The missing region in antitoxin corresponds to the important DBD of HigA. Here we report a 2.09 Å crystal structure of HigBA complex from E. coli K-12 that revealed the electron density for the missing residues in both toxin HigB and antitoxin HigA. Especially, in antitoxin HigA we observed structured DBD, consisting of four helices (α6 to α9) with a compact hydrophobic interior, revealing a complete HigBA complex structure from E. coli K-12 strain. We also report a crystal structure of a truncated, heterodimeric HigBA complex that suggests the possible proteolytic cleavage sites in toxin HigB and antitoxin HigA, which may have implication in HigBA complex regulation in bacteria. We have probed and validated the key putative active site residues using bacterial growth assays. Using gel-mobility shift assays, SEC-MALS, and ITC methods we have probed the interaction of HigBA complex with a 33 bp palindromic DNA sequence from its promoter region. Based on these results, we have generated a model of HigBA – DNA complex that explains the plausible mechanism of transcriptional regulation of HigBA operon expression by HigA. Furthermore, using MD simulations and spectroscopic (CD and NMR) studies, we revealed the intrinsic dynamic and conformational flexibility in HigA homodimer.

Database Depositions

The atomic co-ordinates and structure factors for full length HigBA tetramer and HigBA dimer have been deposited in the Protein Data Bank under PDB accession codes 6KML and 6KMQ respectively.

Abbreviations

HigBA, host inhibition of growth; TA, toxin-antitoxin; NMR, nuclear magnetic resonance; CD, circular dichroism; MD, molecular dynamics; GROMACS, GROningen MAchine for Chemical Simulations.

Author Contributions

M.S. conceived and designed the research; P.V.J, V.K.S. C.K., D.B. and U.R. performed crystallization experiments; P.V.J, V.K.S. M.S. and U.R solved and analyzed the X-ray structures, P.V.J. and V.K.S. performed ITC, and MD simulation experiments. S.C. and R.S. performed growth assays; P.V.J, V.K.S. and M.S. wrote manuscript with inputs from all other authors; all authors reviewed the final manuscript.

Funding

M.S. and R.S acknowledge the financial support received from the Department of Biotechnology (grant number no. BT/COE/34/SP15219/2015). M.S. acknowledges financial support from the Ramalingaswami Fellowship from Department of Biotechnology (DBT), India [BT/RLF/Re-entry/23/2013] and IISc-DBT partnership program.

Acknowledgements

Authors acknowledge Department of Science and Technology and Department of Biotechnology, India for the NMR and ITC facilities at the Indian Institute of Science. Authors acknowledge funding for infrastructural support from the following programs of the Government of India: DST-FIST, UGC-CAS, and the DBT-IISc partnership program. Authors greatly acknowledge the provision of beamtime at the BESSY II electron-storage ring operated by the Helmholtz-Zentrum, Berlin. Authors acknowledge the X-ray diffraction facility for macromolecular crystallography at the Indian Institute of Science used for screening purposes, which is supported by the Department of Science and Technology – Science and Engineering Research Board (DST-SERB) grant IR/SO/LU/0003/2010-PHASE-II. P.V.J. acknowledges the research fellowship from DBT, India. S.C. acknowledges his research fellowship from CSIR, India. R.S. is a recipient of Ramalingaswami Fellowship and National Bioscience Award.

Competing Interests

The authors declare that there are no competing interests associated with the manuscript.

References:

1. Gerdes, K., P.B. Rasmussen, and S. Molin, *Unique type of plasmid maintenance function: postsegregational killing of plasmid-free cells.* Proc Natl Acad Sci U S A, 1986. **83**(10): p. 3116-20.
2. Gotfredsen, M. and K. Gerdes, *The Escherichia coli relBE genes belong to a new toxin-antitoxin gene family.* Mol Microbiol, 1998. **29**(4): p. 1065-76.
3. Ogura, T. and S. Hiraga, *Mini-F plasmid genes that couple host cell division to plasmid proliferation.* Proc Natl Acad Sci U S A, 1983. **80**(15): p. 4784-8.
4. Christensen, S.K., et al., *Overproduction of the Lon protease triggers inhibition of translation in Escherichia coli: involvement of the yefM-yoeB toxin-antitoxin system.* Mol Microbiol, 2004. **51**(6): p. 1705-17.
5. Hayes, F. and L. Van Melderen, *Toxins-antitoxins: diversity, evolution and function.* Crit Rev Biochem Mol Biol, 2011. **46**(5): p. 386-408.
6. Van Melderen, L., P. Bernard, and M. Couturier, *Lon-dependent proteolysis of CcdA is the key control for activation of CcdB in plasmid-free segregant bacteria.* Mol Microbiol, 1994. **11**(6): p. 1151-7.
7. Gerdes, K., et al., *Translational control and differential RNA decay are key elements regulating postsegregational expression of the killer protein encoded by the parB locus of plasmid R1.* Journal of Molecular Biology, 1988. **203**(1): p. 119-129.
8. Dy, R.L., et al., *A widespread bacteriophage abortive infection system functions through a Type IV toxin-antitoxin mechanism.* Nucleic Acids Res, 2014. **42**(7): p. 4590-605.
9. Harms, A., E. Maisonneuve, and K. Gerdes, *Mechanisms of bacterial persistence during stress and antibiotic exposure.* Science, 2016. **354**(6318).
10. Page, R. and W. Peti, *Toxin-antitoxin systems in bacterial growth arrest and persistence.* Nature Chemical Biology, 2016. **12**: p. 208.
11. Harms, A., et al., *Toxins, targets, and triggers: an overview of toxin-antitoxin biology.* Molecular cell, 2018. **70**(5): p. 768-784.
12. Bernard, P., et al., *The F plasmid CcdB protein induces efficient ATP-dependent DNA cleavage by gyrase.* J Mol Biol, 1993. **234**(3): p. 534-41.
13. Overgaard, M., et al., *Messenger RNA interferase RelE controls relBE transcription by conditional cooperativity.* Mol Microbiol, 2008. **69**(4): p. 841-57.
14. Motiejunaite, R., et al., *Escherichia coli dinJ-yafQ genes act as a toxin-antitoxin module.* FEMS Microbiol Lett, 2007. **268**(1): p. 112-9.
15. Jiang, Y., et al., *ParE toxin encoded by the broad-host-range plasmid RK2 is an inhibitor of Escherichia coli gyrase.* Mol Microbiol, 2002. **44**(4): p. 971-9.
16. Pedersen, K., et al., *The bacterial toxin RelE displays codon-specific cleavage of mRNAs in the ribosomal A site.* Cell, 2003. **112**(1): p. 131-40.
17. Zhang, Y., et al., *MazF cleaves cellular mRNAs specifically at ACA to block protein synthesis in Escherichia coli.* Mol Cell, 2003. **12**(4): p. 913-23.
18. Zhang, Y. and M. Inouye, *The inhibitory mechanism of protein synthesis by YoeB, an Escherichia coli toxin.* J Biol Chem, 2009. **284**(11): p. 6627-38.
19. Hurley, J.M. and N.A. Woychik, *Bacterial toxin HigB associates with ribosomes and mediates translation-dependent mRNA cleavage at A-rich sites.* J Biol Chem, 2009. **284**(28): p. 18605-13.
20. Yamaguchi, Y., J.H. Park, and M. Inouye, *MqsR, a crucial regulator for quorum sensing and biofilm formation, is a GCU-specific mRNA interferase in Escherichia coli.* J Biol Chem, 2009. **284**(42): p. 28746-53.
21. Zhang, Y., et al., *Insights into the mRNA cleavage mechanism by MazF, an mRNA interferase.* J Biol Chem, 2005. **280**(5): p. 3143-50.
22. Ruangprasert, A., et al., *Molecular basis of ribosome recognition and mRNA hydrolysis by the E. coli YafQ toxin.* Nucleic Acids Research, 2015. **43**(16): p. 8002-8012.

23. Prysak, M.H., et al., *Bacterial toxin YafQ is an endoribonuclease that associates with the ribosome and blocks translation elongation through sequence-specific and frame-dependent mRNA cleavage.* Mol Microbiol, 2009. **71**(5): p. 1071-87.
24. Tian, Q.B., et al., *A new plasmid-encoded proteic killer gene system: cloning, sequencing, and analyzing hig locus of plasmid Rts1.* Biochem Biophys Res Commun, 1996. **220**(2): p. 280-4.
25. Christensen‐Dalsgaard, M., M.G. Jørgensen, and K. Gerdes, *Three new RelE‐homologous mRNA interferases of Escherichia coli differentially induced by environmental stresses.* Molecular microbiology, 2010. **75**(2): p. 333-348.
26. Yang, J., et al., *Structural insight into the E. coli HigBA complex.* Biochemical and biophysical research communications, 2016. **478**(4): p. 1521-1527.
27. Xu, B.-S., et al., *Conformational changes of antitoxin HigA from Escherichia coli str. K-12 upon binding of its cognate toxin HigB reveal a new regulation mechanism in toxin-antitoxin systems.* Biochemical and biophysical research communications, 2019. **514**(1): p. 37-43.
28. Yoon, W.-S., et al., *Structural changes of antitoxin HigA from Shigella flexneri by binding of its cognate toxin HigB.* International journal of biological macromolecules, 2019. **130**: p. 99-108.
29. Powell, H.R., et al., *Integrating macromolecular X-ray diffraction data with the graphical user interface iMosflm.* Nature protocols, 2017. **12**(7): p. 1310.
30. Battye, T.G.G., et al., *iMOSFLM: a new graphical interface for diffraction-image processing with MOSFLM.* Acta Crystallographica Section D: Biological Crystallography, 2011. **67**(4): p. 271-281.
31. Kabsch, W., *Xds.* Acta Crystallographica Section D: Biological Crystallography, 2010. **66**(2): p. 125-132.
32. Emsley, P., et al., *Features and development of Coot.* Acta Crystallographica Section D: Biological Crystallography, 2010. **66**(4): p. 486-501.
33. Afonine, P.V., et al., *Towards automated crystallographic structure refinement with phenix. refine.* Acta Crystallographica Section D: Biological Crystallography, 2012. **68**(4): p. 352-367.
34. Chen, V.B., et al., *MolProbity: all-atom structure validation for macromolecular crystallography.* Acta Crystallographica Section D: Biological Crystallography, 2010. **66**(1): p. 12-21.
35. Abraham, M.J., et al., *GROMACS: High performance molecular simulations through multi-level parallelism from laptops to supercomputers.* SoftwareX, 2015. **1**: p. 19-25.
36. Schmid, N., et al., *Definition and testing of the GROMOS force-field versions 54A7 and 54B7.* European biophysics journal, 2011. **40**(7): p. 843.
37. Hess, B., *P-LINCS: A Parallel Linear Constraint Solver for Molecular Simulation.* J Chem Theory Comput, 2008. **4**(1): p. 116-22.
38. Xu, B.S., et al., *Conformational changes of antitoxin HigA from Escherichia coli str. K-12 upon binding of its cognate toxin HigB reveal a new regulation mechanism in toxin-antitoxin systems.* Biochem Biophys Res Commun, 2019. **514**(1): p. 37-43.
39. Amadei, A., A.B. Linssen, and H.J. Berendsen, *Essential dynamics of proteins.* Proteins: Structure, Function, and Bioinformatics, 1993. **17**(4): p. 412-425.
40. David, C.C. and D.J. Jacobs, *Principal component analysis: a method for determining the essential dynamics of proteins*, in *Protein dynamics*. 2014, Springer. p. 193-226.
41. Maisuradze, G.G. and D.M. Leitner, *Free energy landscape of a biomolecule in dihedral principal component space: Sampling convergence and correspondence between structures and minima.* Proteins: Structure, Function, and Bioinformatics, 2007. **67**(3): p. 569-578.
42. Pettersen, E.F., et al., *UCSF Chimera—a visualization system for exploratory research and analysis.* Journal of computational chemistry, 2004. **25**(13): p. 1605-1612.
43. van Dijk, M. and A.M. Bonvin, *3D-DART: a DNA structure modelling server.* Nucleic acids research, 2009. **37**(suppl_2): p. W235-W239.
44. Hornak, V., et al., *Comparison of multiple Amber force fields and development of improved protein backbone parameters.* Proteins, 2006. **65**(3): p. 712-25.

45. Abraham, M.J., et al., *GROMACS: High performance molecular simulations through multi-level parallelism from laptops to supercomputers.* SoftwareX, 2015. **1-2**: p. 19-25.
46. Krishnamoorthy, G.K., et al., *Isothermal titration calorimetry and surface plasmon resonance analysis using the dynamic approach.* Biochem Biophys Rep, 2020. **21**: p. 100712.
47. Jen-Jacobson, L., L.E. Engler, and L.A. Jacobson, *Structural and thermodynamic strategies for site-specific DNA binding proteins.* Structure, 2000. **8**(10): p. 1015-23.
48. Schureck, M.A., et al., *Structural basis of transcriptional regulation by the HigA antitoxin.* Molecular microbiology, 2019. **111**(6): p. 1449-1462.
49. Aggarwal, A.K., et al., *Recognition of a DNA operator by the repressor of phage 434: a view at high resolution.* Science, 1988. **242**(4880): p. 899-907.
50. Talavera, A., et al., *A dual role in regulation and toxicity for the disordered N-terminus of the toxin GraT.* Nat Commun, 2019. **10**(1): p. 972.
51. Neubauer, C., et al., *The structural basis for mRNA recognition and cleavage by the ribosome-dependent endonuclease RelE.* Cell, 2009. **139**(6): p. 1084-1095.
52. Yang, Q.E. and T.R. Walsh, *Toxin–antitoxin systems and their role in disseminating and maintaining antimicrobial resistance.* FEMS microbiology reviews, 2017. **41**(3): p. 343-353.
53. Schureck, M.A., et al., *Defining the mRNA recognition signature of a bacterial toxin protein.* Proceedings of the National Academy of Sciences, 2015. **112**(45): p. 13862-13867.
54. Muthuramalingam, M., J.C. White, and C.R. Bourne, *Toxin-antitoxin modules are pliable switches activated by multiple protease pathways.* Toxins, 2016. **8**(7): p. 214.
55. LeRoux, M., et al., *Stress Can Induce Transcription of Toxin-Antitoxin Systems without Activating Toxin.* Mol Cell, 2020. **79**(2): p. 280-292 e8.
56. Snyder, D.A., et al., *Comparisons of NMR spectral quality and success in crystallization demonstrate that NMR and X-ray crystallography are complementary methods for small protein structure determination.* J Am Chem Soc, 2005. **127**(47): p. 16505-11.
57. Yee, A.A., et al., *NMR and X-ray crystallography, complementary tools in structural proteomics of small proteins.* J Am Chem Soc, 2005. **127**(47): p. 16512-7.
58. Zhang, S.-P., et al., *Type II toxin–antitoxin system in bacteria: activation, function, and mode of action.* Biophysics Reports, 2020. **6**(2): p. 68-79.
59. Harms, A., E. Maisonneuve, and K. Gerdes, *Mechanisms of bacterial persistence during stress and antibiotic exposure.* Science, 2016. **354**(6318): p. aaf4268.

Figure legends

Figure 1. 2.09 Å resolution crystal structure of tetrameric HigBA complex from E. coli K12. A) A crystal structure of tetrameric HigBA complex determined in this study (PDB 6KML). The antitoxin protomers are in cyan ribbons and the toxin HigB protomers are in orange. B) Overlay of current HigBA structure (HigB in orange and HigA in blue) and a previously determined structure (PDB 5IFG, in grey) depicting the differences in the two structures. The red circles highlight the missing residues and the unstructured helix (α8) in antitoxin HigA structure (PDB 5IFG). These regions are well defined in the electron density in the current structure. C) Sequence alignment of antitoxin HigA in PDB 6KML and PDB 5IFG with the helices depicted as bars on top of the sequence. The C-terminal DBD region with well-defined secondary structures (helices α8 and α9) in the current structure is highlighted in a green box.

Figure 2. The DNA binding domain (DBD) of *E. coli* K12 HigA from HigBA TA complex. A) Cartoon representation of C-terminal DBD of antitoxin HigA. Four helices are marked from α6-α9. Two loops L1 (connecting α6 and α7) and L2 (connecting α7 and α8) are marked. B) Overlay of DBDs from *E. coli* K12 HigA (red), *P. vulgaris* HigA (pink), and phage 434 repressor protein (green).

Figure 3. Interaction of E. coli HigBA with dsDNA from its promoter region. A) Oligomeric state and molecular weight analysis of HigBA complex (black) and HigBA – DNA complex (red) using SEC-MALS. SEC –MALS analysis revealed a molecular weight ~51 kDa for HigBA that corresponds to the expected molecular weight of a tetrameric complex. A molecular weight of ~116 kDa for HigBA - Pal-1 DNA was revealed by SEC-MALS analysis that corresponds to a stoichiometry of 1:2 (One Pal-1 DNA and two HigBA tetramers). B-C) Interaction of antitoxin HigA dimer (B) and HigBA heterotetramer (C) with Pal-1 DNA probed using ITC. Raw and fitted ITC isotherms are shown. Calculated dissociation constant (K_D) are mentioned in the figures. D) Proposed model of E. coli HigBA tetramer bound to the 33 bp Pal-1 DNA from its promoter region. The sequence of the 33 bp Pal-1 DBD is shown with the inverted repeat sequence highlighted in brown (both in the model and sequence). There are two HigBA tetramers bound to one Pal-1 DNA molecule in the model. In a HigBA tetramer, two protomers of antitoxin bind to the major grove of DNA using the C-terminal DBD. HigA DBD is shown in green and rest of the HigA is shown in blue. The α-helices in DBD are marked in one HigA protomer. Toxin HigB is shown in orange.

Figure 4. 2.30 Å resolution crystal structure of dimeric HigBA complex from E. coli K12. A) A cartoon representation of dimeric HigBA complex determined in this study. The truncated toxin HigB is shown in pink and truncated antitoxin HigA is shown in light blue with secondary structure elements marked. B) Overlay of tetrameric (in grey) and dimeric (blue and pink) HigBA structures highlighting the differences in the two structures. The dimeric HigBA lacks the N-terminal dimerization domain (green) in antitoxin HigA and lacks the C-terminal helix α4 (orange) in the toxin HigB. C-D) Sequence alignment of toxin HigB (C) and antitoxin HigA (D) protomers from tetrameric and dimeric HigBA complexes. The missing residues in dimeric HigBA are shown in color.

Figure 5. Functional characterization of toxin HigB and its mutants. A) The location of selected putative active site residues (in blue sticks) and C-terminal helix α4 (in red) are shown on the HigB structure. B) Monitoring the growth of E. coli BL-21 (pLys, DE3)

transformed with empty vector and vector encoding HigB, HigB-Δα4, HigB-D49A/N50A, and HigB-R68A. The expression was induced by addition of 1 mM IPTG and bacterial growth was monitored by measuring optical density of culture at 600 nm wavelength at indicated time points. C, D) Spotting assays was performed to monitor bacterial growth on solid LB agar plates. Monitoring growth of vector only and mutant HigB containing bacterial cultures, 10-fold serial dilutions of induced (5 h post induction) (C) and uninduced (at zero time) (D) cultures were prepared and spotted on LB Agar plates. The numbers represent the dilution of the spot with 1 representing lowest dilution and 6 representing highest dilution. The plates were incubated at 37 ^{o}C overnight and images were recorded. Growth of a bacterial culture that contains empty vector is monitored in both the experiments as a control. The data shown in these panels is representative of three independent experiments.

Figure 6. MD simulation study of HigBA complex. A) RMSD plot of HigBA complex (black) and HigB (green) and HigA (red) extracted from the trajectories of 100 ns MD simulations of HigBA complex. B, C) Two dimensional (B) and three dimensional (3) FEL contour map of HigBA complex. The red, green, and blue triangles (in B) represent three minima locations from which the structures were extracted for further analysis. D) Overlay of three FEL minimum energy representative structures (red, green and blue) of toxin HigB with the initial structure (in grey). E) Overlay of three FEL minimum energy representative structures (red, green and blue) of antitoxin HigA homodimer with the initial structure (in grey).

Figure 7. Characterization of antitoxin HigA homodimer in solution. A) A CD spectrum of HigA, showing that the protein is α-helical in solution. B) Thermal melting of HigA dimer monitored using CD spectroscopy. A calculated melting temperature (Tm) of 57 ℃ is mentioned in the figure. C) A 2D ^{1}H-^{15}N TROSY HSQC NMR spectrum of full-length HigA homodimer.

Figure 8. Comparison of antitoxin HigA in free and HigBA bound conformations. The line representation of structures in blue, red and green represent E. coli HigA homodimer from free HigA structure (PDB 6JQ4), HigBA tetramer structure reported here (PDB 6KML), and HigBA tetramer structure solved earlier (PDB 5IFG). Distances measured at three locations along the structures are marked in the figure.

Tables

Table 1. Crystallographic data collection and structure refinement statistics

Table 2. Equilibrium dissociation constants (KDs) and other thermodynamic parameters derived for the HigA homodimer – DNA and HigBA tetramer – DNA interactions using ITC experiments.

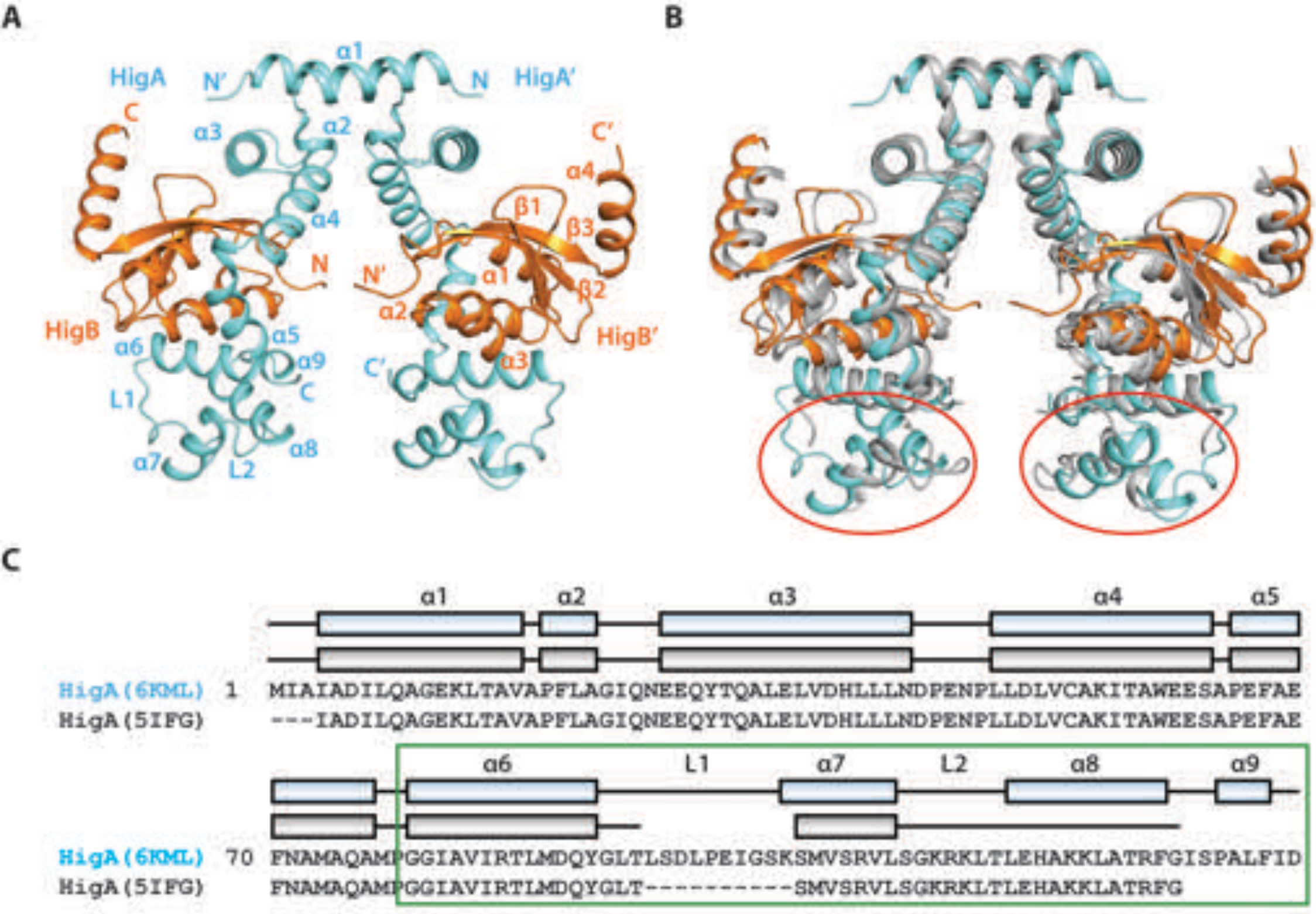
A
HigA
N'
α1
N
HigA'
C
α3
α2
C'
α4
β1
α4
β3
N
N'
α1
β2
α2
HigB
HigB'
α6
α5
α9
C'
α3
C
L1
α8
α7
L2
B
C
α1
α2
α3
α4
α5
HigA(6KML) 1 MIAIADILQAGEKLTAVAPFLAGIQNEEQYTQALELVDHLLLNDPENPLLDLVCAKITAWEESAPEFAE
HigA(5IFG) ---IADILQAGEKLTAVAPFLAGIQNEEQYTQALELVDHLLLNDPENPLLDLVCAKITAWEESAPEFAE
α6
L1
α7
L2
α8
α9
HigA(6KML) 70 FNAMAQAMPGGIAVIRTLMDQYGLTLSDLPEIGSKSMVSRVLSGKRKLTLEHAKKLATRFGISPALFID
HigA(5IFG) FNAMAQAMPGGIAVIRTLMDQYGLT----------SMVSRVLSGKRKLTLEHAKKLATRFG

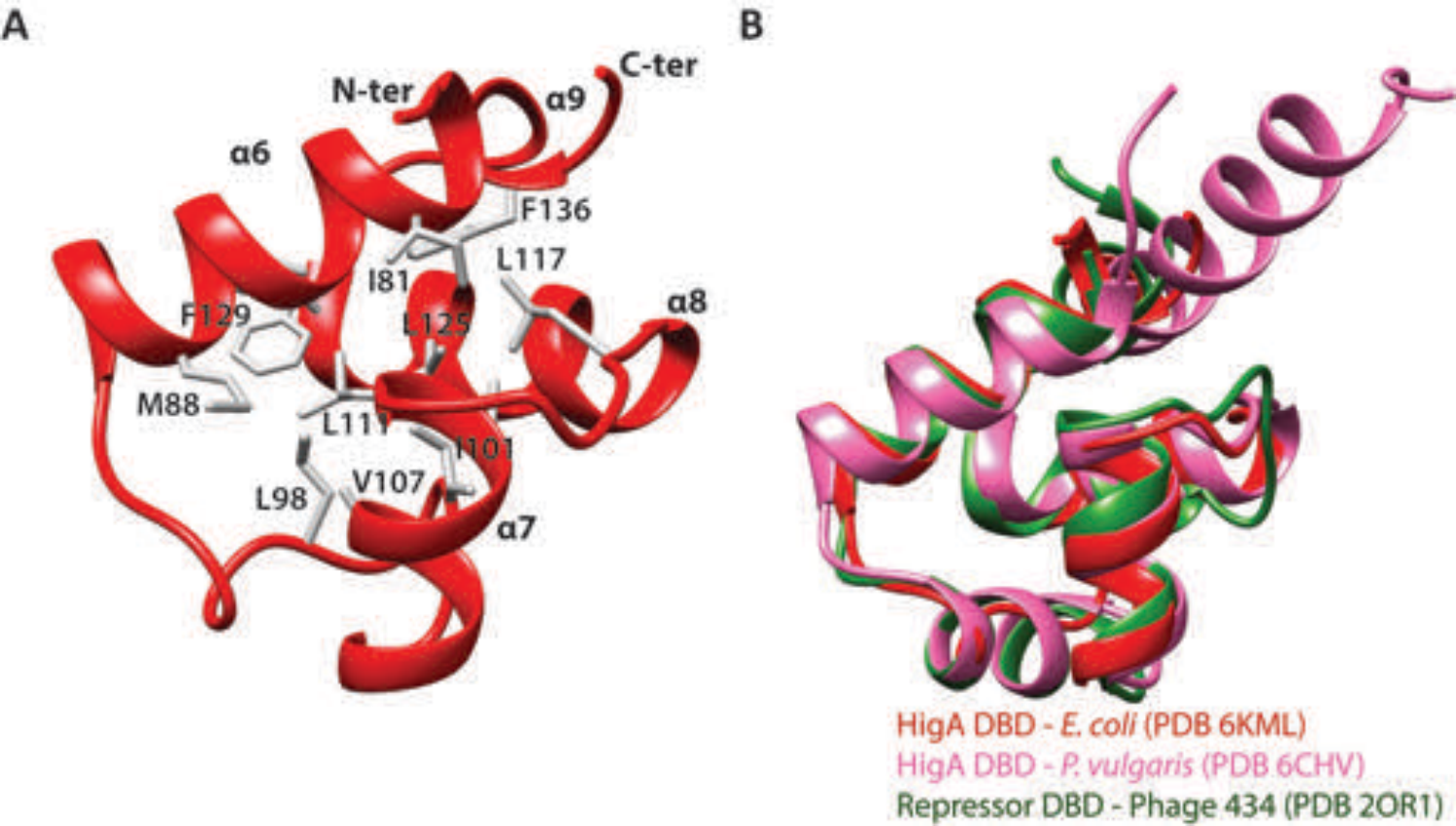
A
N-ter
α9
C-ter
α6
F136
I81
L117
F129
L125
α8
M88
L111
I101
L98
V107
α7
B
HigA DBD - E. coli (PDB 6KML)
HigA DBD - P. vulgaris (PDB 6CHV)
Repressor DBD - Phage 434 (PDB 2OR1)

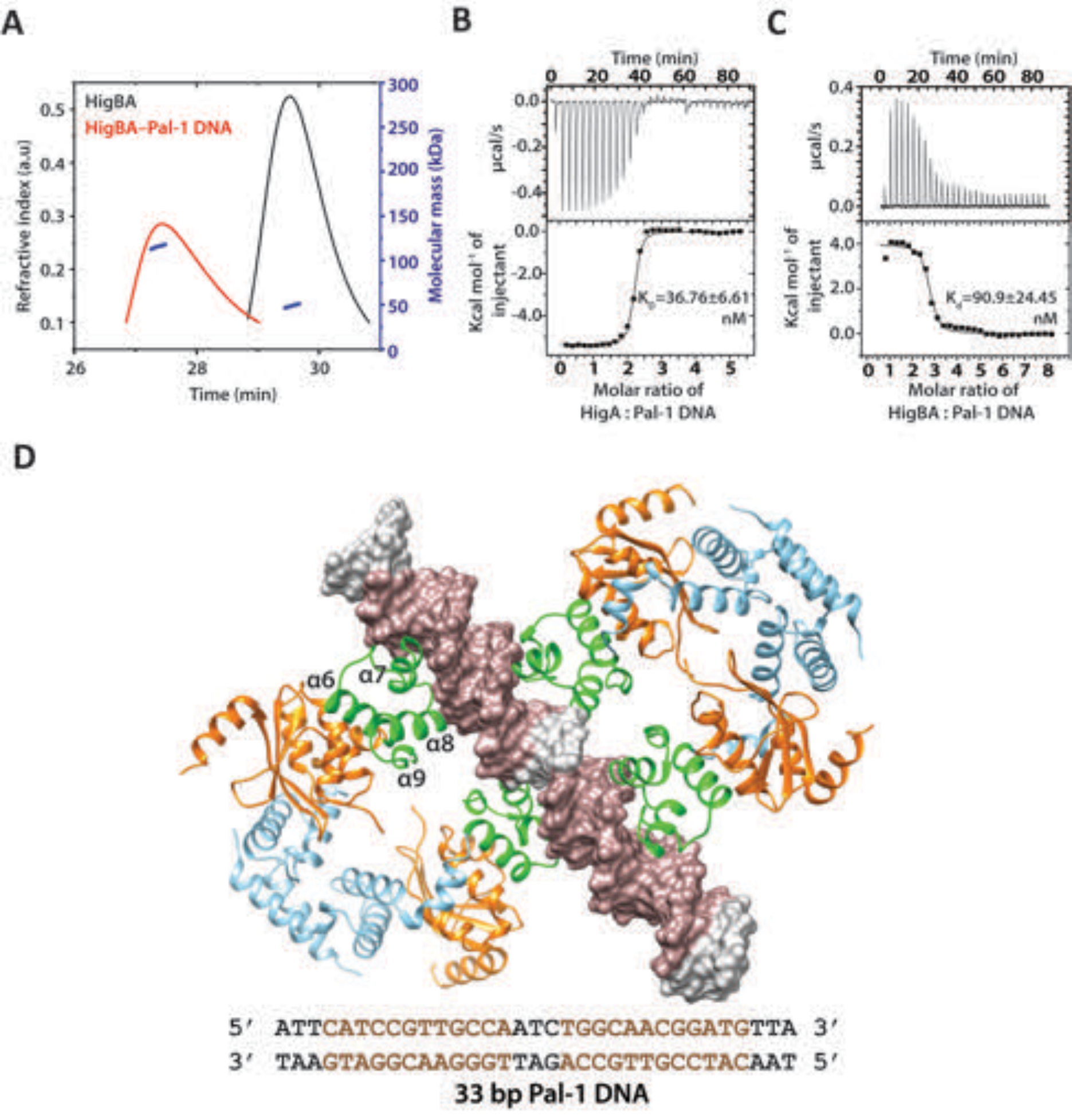
A
HigBA
HigBA–Pal-1 DNA
Refractive index (a.u)
Molecular mass (kDa)
Time (min)
B
Time (min)
µcal/s
Kcal mol⁻¹ of injectant
K_D=36.76±6.61 nM
Molar ratio of HigA : Pal-1 DNA
C
Time (min)
µcal/s
Kcal mol⁻¹ of injectant
K_d=90.9±24.45 nM
Molar ratio of HigBA : Pal-1 DNA
D
α6
α7
α8
α9
5′ ATTCATCCGTTGCCAATCTGGCAACGGATGTTA 3′
3′ TAAGTAGGCAAGGGTTAGACCGTTGCCTACAAT 5′
33 bp Pal-1 DNA

A

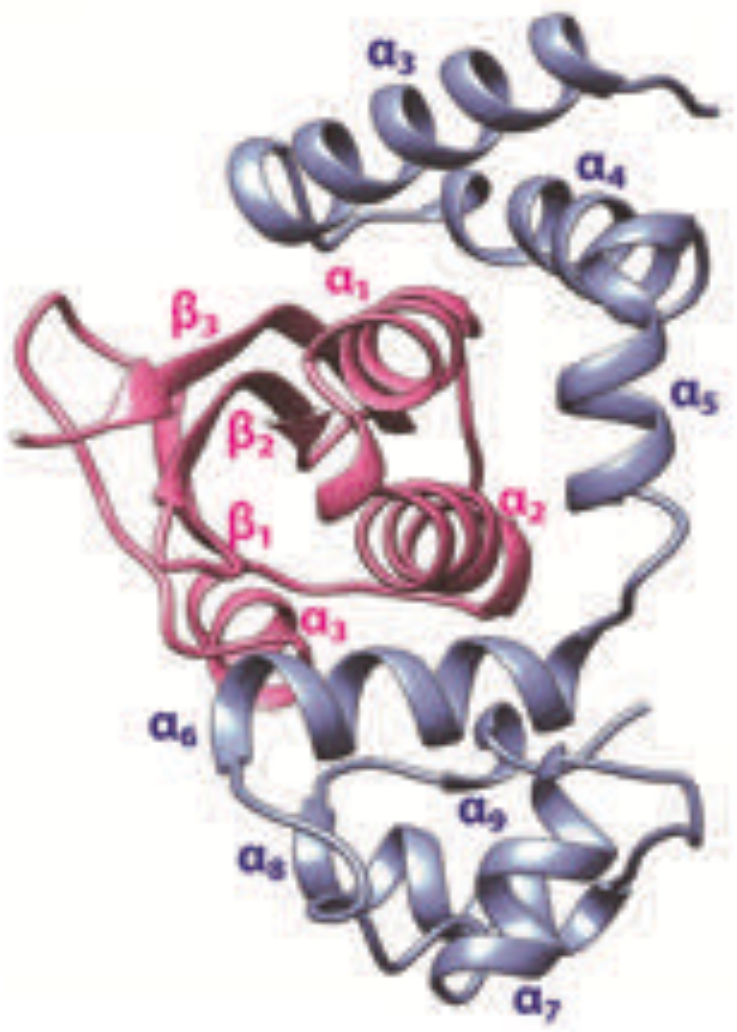
α3
α4
α1
β3
α5
β2
α2
β1
α3
α6
α9
α8
α7

B

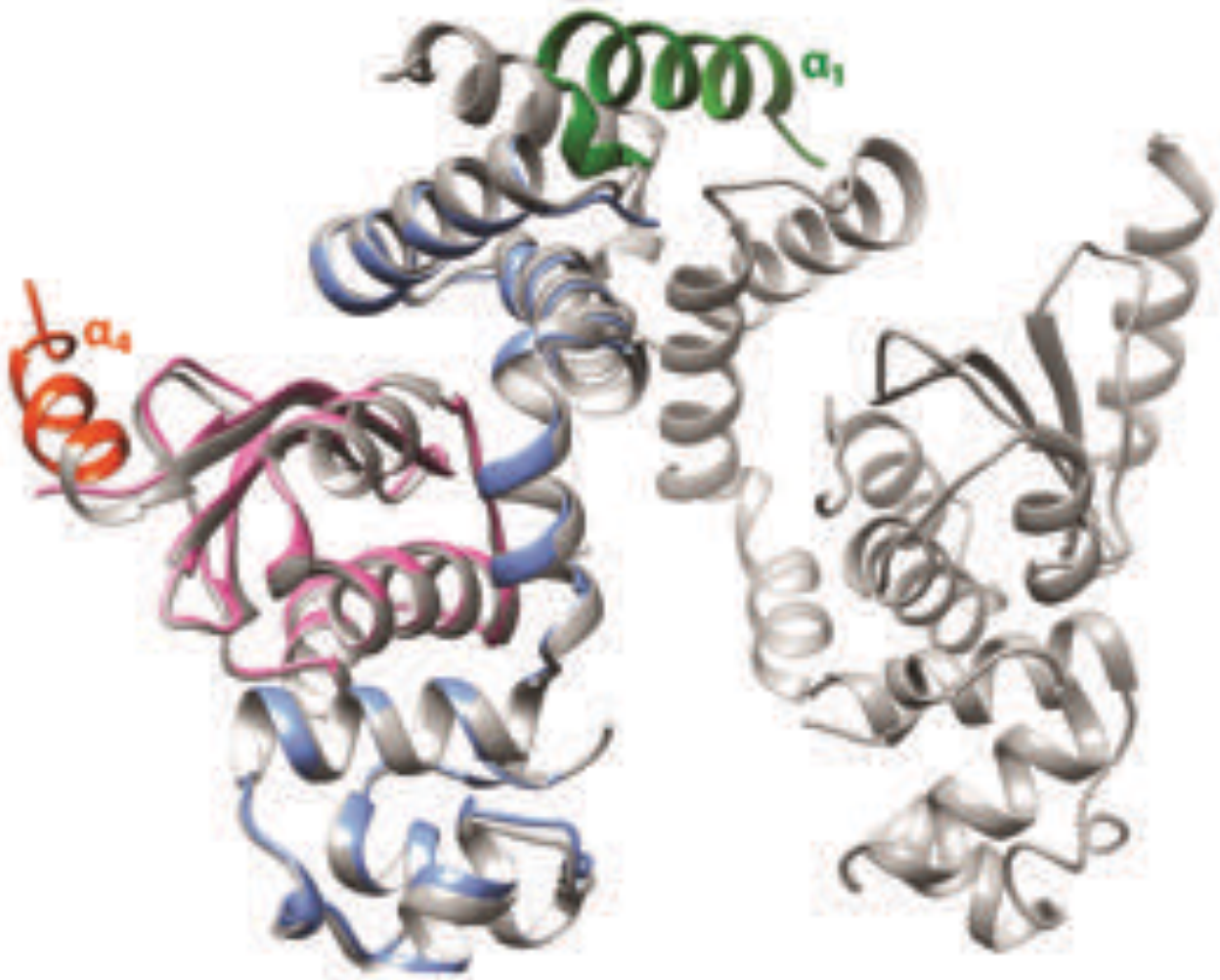
α1
α4

C

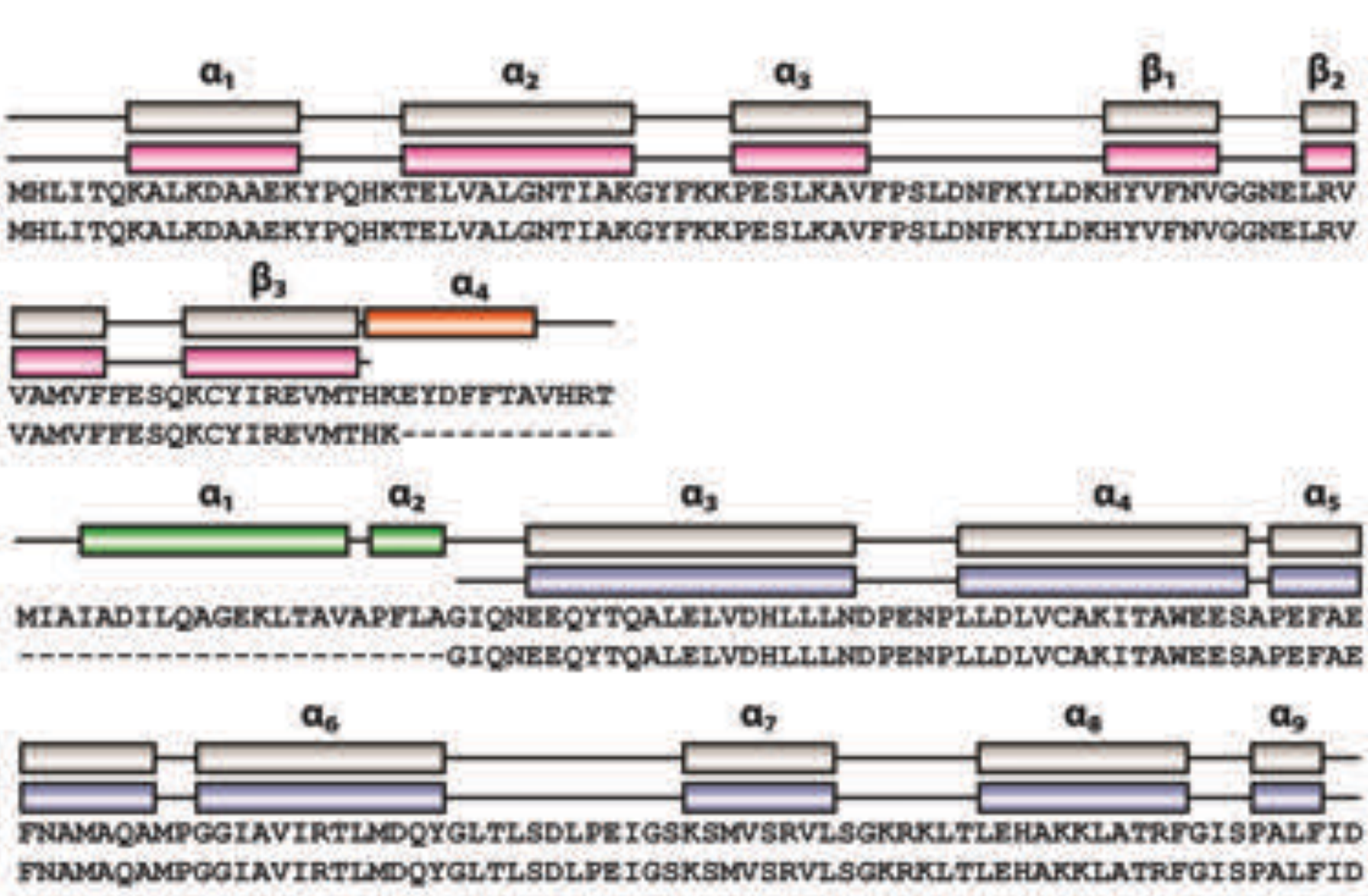
α1 α2 α3 β1 β2
HigB(6KML) 1 MHLITQKALKDAAEKYPQHKTELVALGNTIAKGYFKKPESLKAVFPSLDNFKYLDKHYVFNVGGNELRV
HigB(6KMQ) 1 MHLITQKALKDAAEKYPQHKTELVALGNTIAKGYFKKPESLKAVFPSLDNFKYLDKHYVFNVGGNELRV
β3 α4
HigB(6KML) 70 VAMVFFESQKCYIREVMTHKEYDFFTAVHRT
HigB(6KMQ) 70 VAMVFFESQKCYIREVMTHK----------
α1 α2 α3 α4 α5
HigA(6KML) 1 MIAIADILQAGEKLTAVAPFLAGIQNEEQYTQALELVDHLLLNDPENPLLDLVCAKITAWEESAPEFAE
HigA(6KMQ) ----------GIQNEEQYTQALELVDHLLLNDPENPLLDLVCAKITAWEESAPEFAE
α6 α7 α8 α9
HigA (6KML) 70 FNAMAQAMPGGIAVIRTLMDQYGLTLSDLPEIGSKSMVSRVLSGKRKLTLEHAKKLATRFGISPALFID
HigA (6KMQ) FNAMAQAMPGGIAVIRTLMDQYGLTLSDLPEIGSKSMVSRVLSGKRKLTLEHAKKLATRFGISPALFID

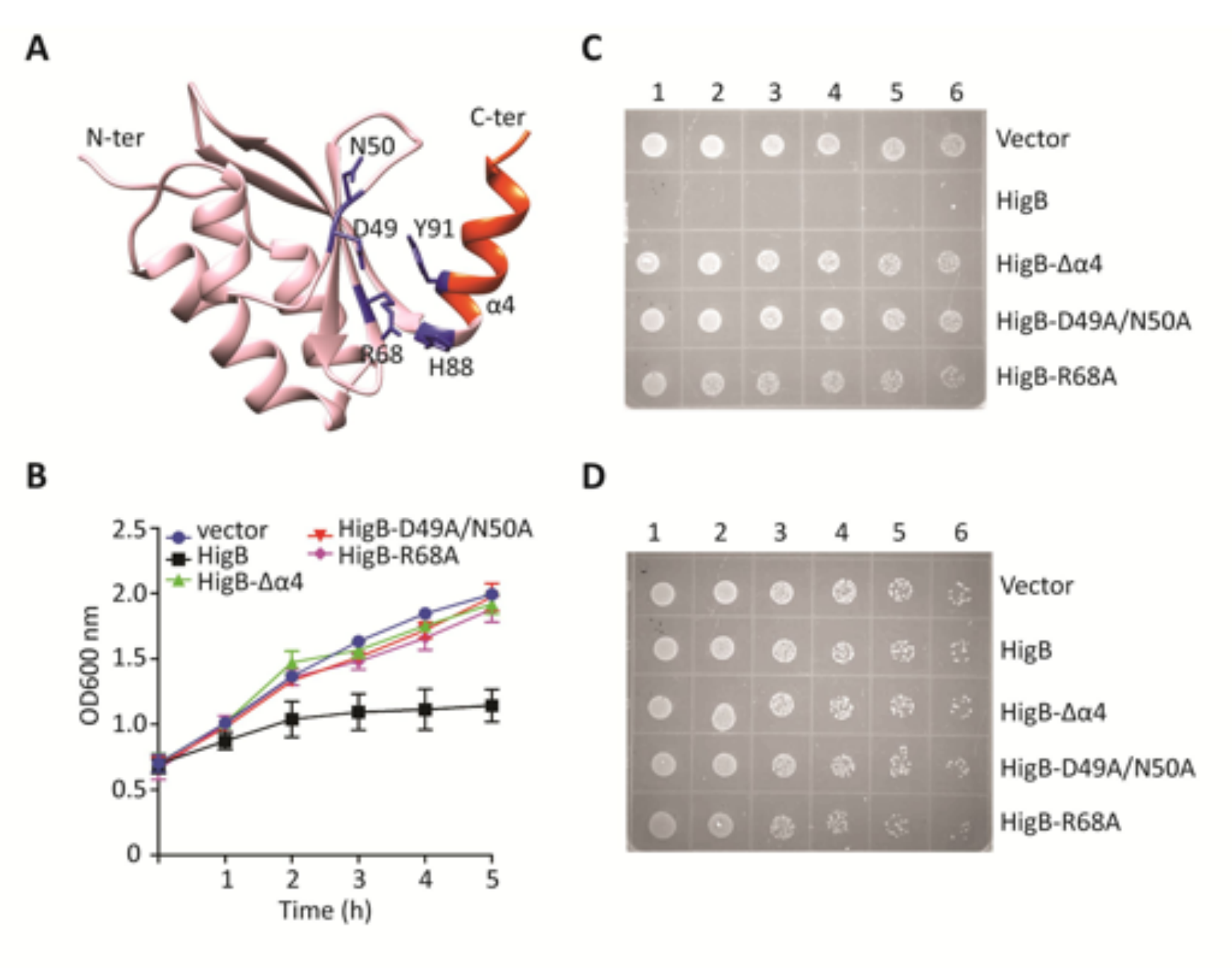
A
N-ter
C-ter
N50
D49
Y91
α4
R68
H88
B
vector
HigB
HigB-Δα4
HigB-D49A/N50A
HigB-R68A
OD600 nm
Time (h)
C
1 2 3 4 5 6
Vector
HigB
HigB-Δα4
HigB-D49A/N50A
HigB-R68A
D
1 2 3 4 5 6
Vector
HigB
HigB-Δα4
HigB-D49A/N50A
HigB-R68A

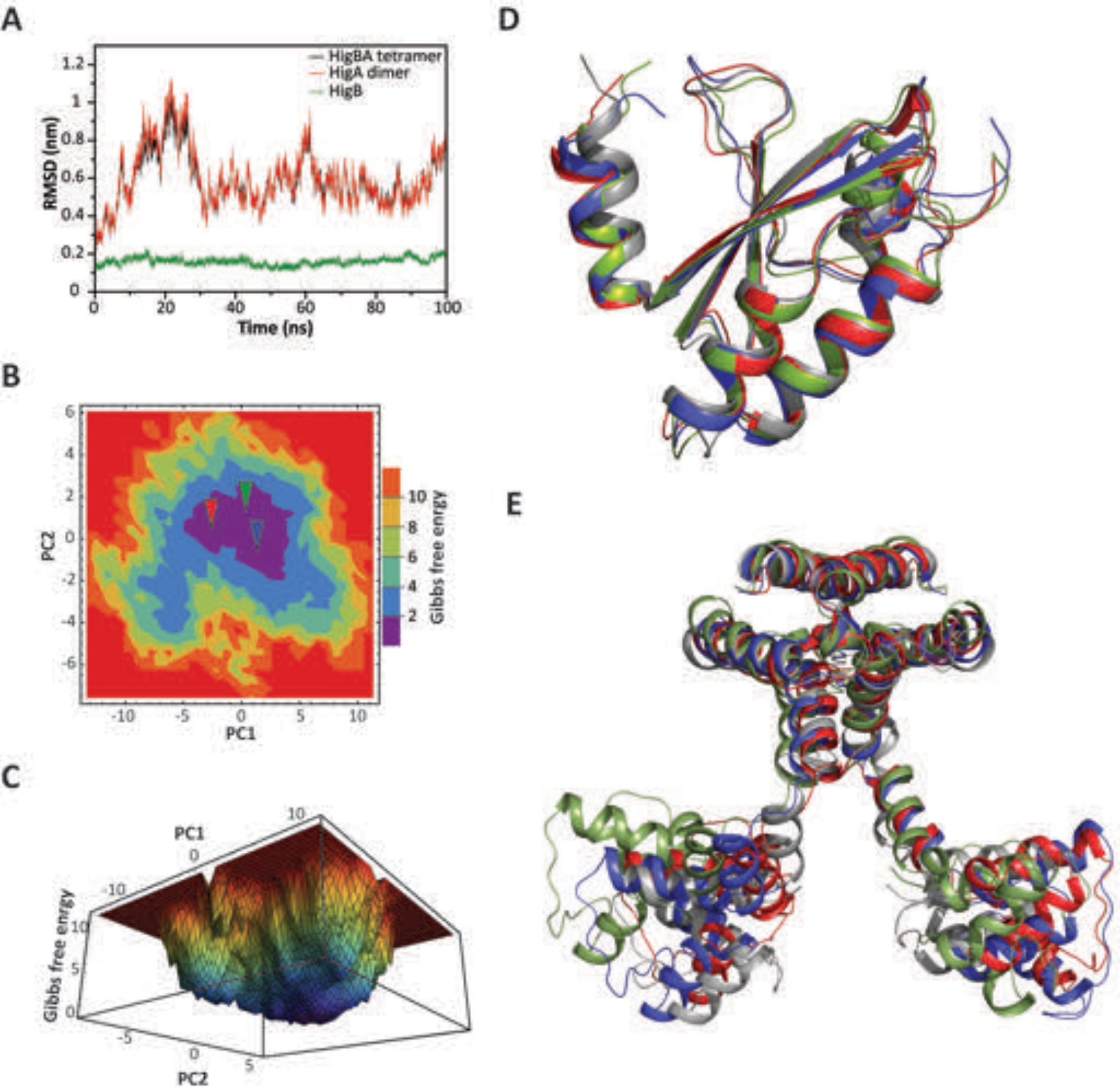
A
HigBA tetramer
HigA dimer
HigB
RMSD (nm)
Time (ns)
B
PC2
PC1
Gibbs free energy
C
PC1
PC2
Gibbs free energy
D
E

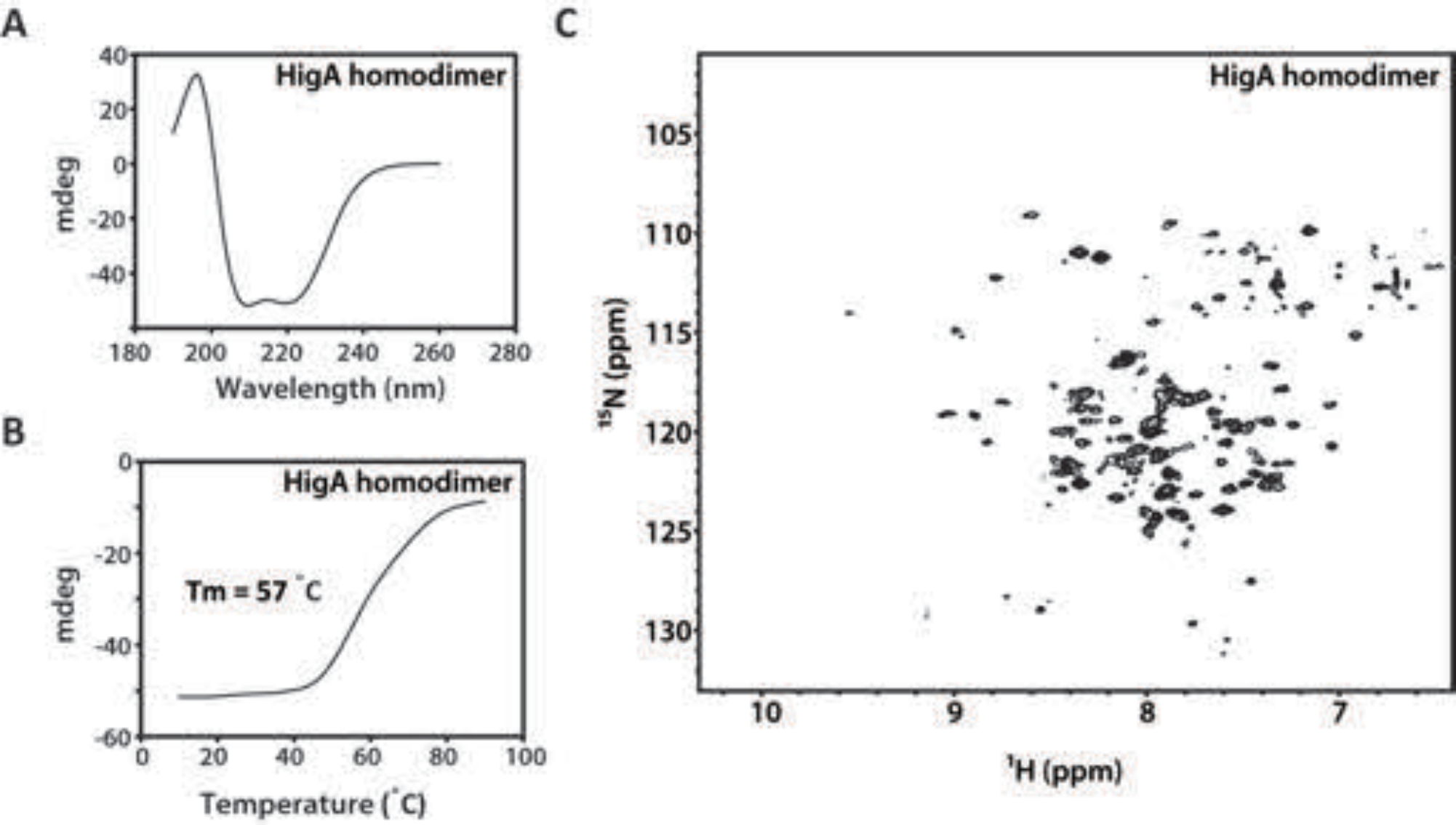
A
HigA homodimer
mdeg
40
20
0
-20
-40
180
200
220
240
260
280
Wavelength (nm)
B
HigA homodimer
Tm = 57 °C
mdeg
0
-20
-40
-60
0
20
40
60
80
100
Temperature (°C)
C
HigA homodimer
105
110
115
120
125
130
15N (ppm)
10
9
8
7
1H (ppm)

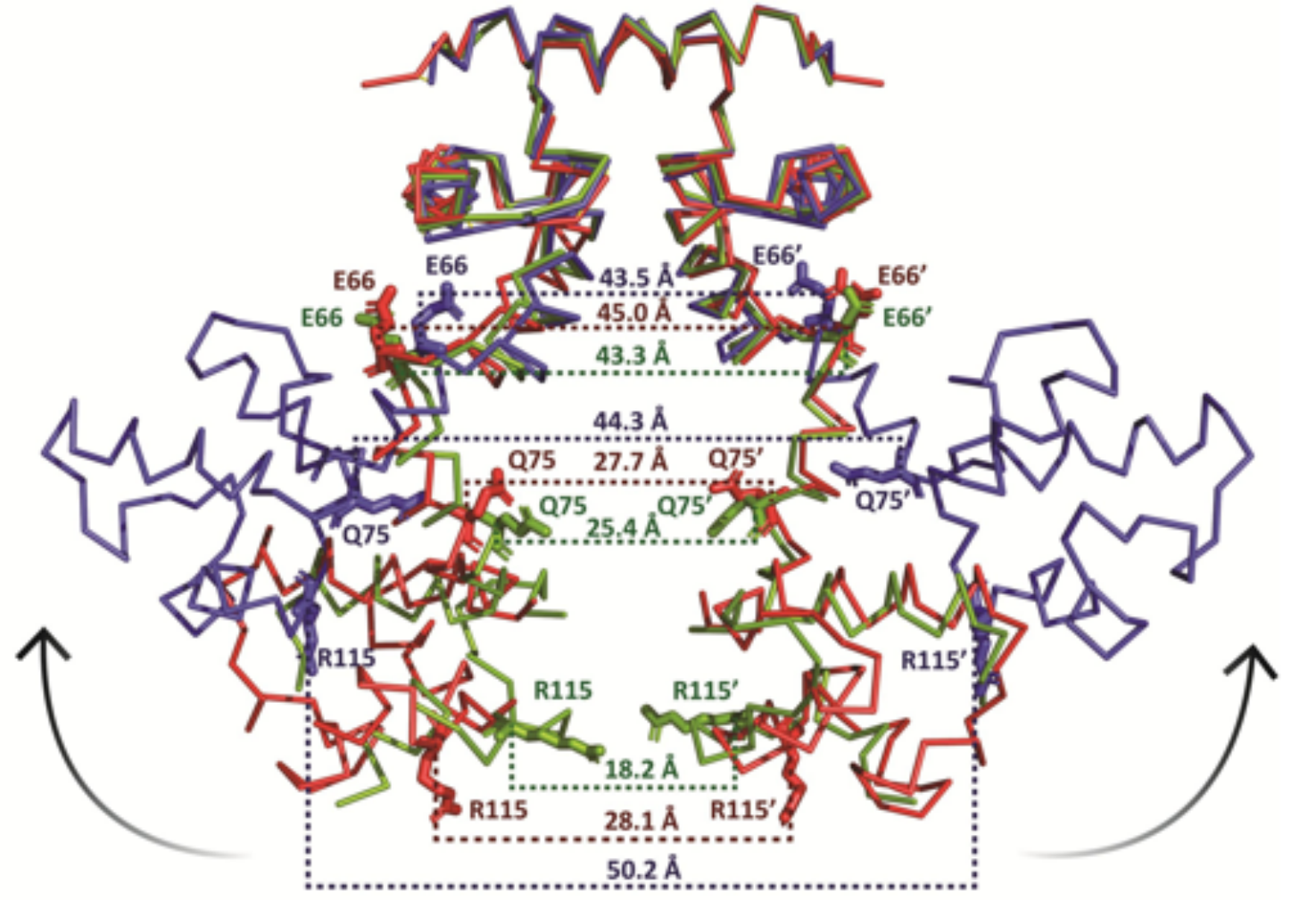
E66
E66
43.5 Å
E66'
E66'
E66
45.0 Å
E66'
43.3 Å
44.3 Å
Q75
27.7 Å
Q75'
Q75
Q75'
Q75'
Q75
25.4 Å
R115
R115
R115'
R115'
18.2 Å
R115
28.1 Å
R115'
50.2 Å

Table 1. Crystallographic data collection and structure refinement statistics

	HigBA tetramer	**HigBA dimer**
PDB code	6KML	6KMQ
Integration		
Space group	P 1 21 1	P 1 21 1
Cell constants	a = 57.387Å, b = 85.87Å, c = 59.41Å α = 90.00◦, β = 90.85◦, γ = 90.00◦	a = 37.96Å, b = 48.27Å, c = 56.07Å α = 90.00°, β = 100.82°, γ = 90.00°
Wavelength (Å)	0.9184	0.9184
Observed reflections	39733	33043
Unique reflections	12111	8815
CC(1/2)	99.9	99.9
% Data completeness (in resolution range)	96.3 (48.85-2.09)	97.17 (28.49-2.3)
< I/σ(I) >	1.25 (at 2.09Å)	1.36 (at 2.3Å)
Resolution range (Å)	48.85 - 2.09	28.49 - 2.3
Refinement		
R_{work}, R_{free}	0.195, 0.236	0.260, 0.297
R free test set	1649 reflections (5.00%)	420 reflections (5.12%)
Average B, all atoms (Å2)	41.61	50.4
R.m.s.d bond length (Å)/ angles (°)	0.008/ 0.931	0.002/ 0.394
Total number of atoms	Total: 3976 Solvent: 197 Non-solvent: 3779	Total: 1566 Solvent: 0 Non-solvent: 1566
Ramachandran outliers Favored/allowed/outliers (%)	99/1/0	97.04/2.96/0
MolProbity Clash score (percentile rank)	5.65 (97^{th})	4.51 (99^{th})

Table 2. Equilibrium dissociation constants (K_Ds) and other thermodynamic parameters derived for the HigA homodimer – DNA and HigBA tetramer – DNA interactions using ITC experiments

Experiment	**K_D (nM)**	**ΔG (kcal/mol)**	**ΔH (kcal/mol)**	**TΔS (kcal/mol)**	**n**
HigA homodimer **–** Pal-1 DNA	36.76±6.61	-10.32±1.85	-5.38±0.04	4.94±0.92	2.13±0.01
HigBA heteroteramer **–** Pal-1 DNA	90.9±24.45	-9.77±2.62	3.96±0.08	13.73±3.97	2.17±0.02

Supplementary information

2.09 Å resolution structure of *E. coli* HigBA toxin-antitoxin complex reveals an ordered DNA-binding domain and intrinsic dynamics in antitoxin

Pankaj Vilas Jadhav[1,$], Vikrant Kumar Sinha[1,$], Saurabh Chugh[3], Chaithanya Kotyada[1, 5], Digvijay Bachhav[1,6], Ramandeep Singh[3], Ulli Rothweiler[4,*], and Mahavir Singh[1,2,*]

[$] Equal contribution

* To whom correspondence should be addressed:

Email: ulli.rothweiler@uit.no (U.R.); singh@iisc.ac.in (M.S.)

This file contains:

Supplementary Figures S1-S6

A

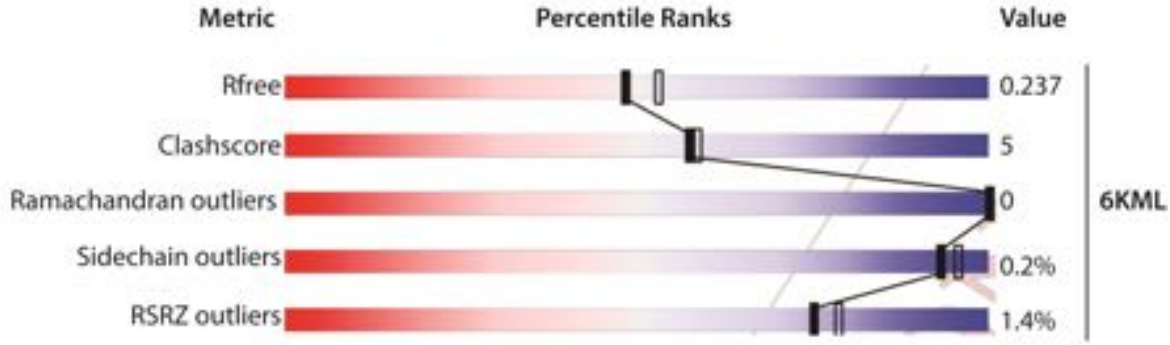

B

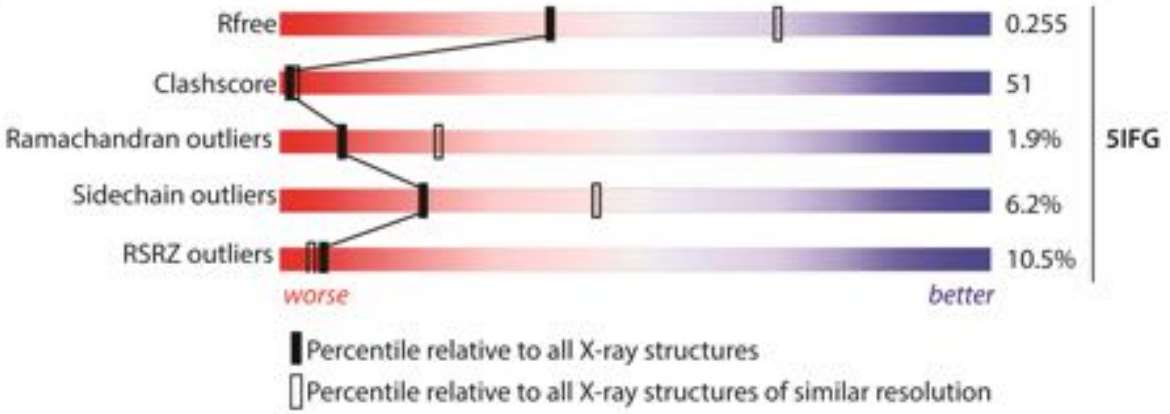

C

	PDB 6KML	PDB 5IFG
Crystallization condition	0.2M KCl, 0.05M Tris-Cl pH (7.5),15% PEG 3350 + 0.05M MgCl2	0.2M (NH4)2SO4, 0.1M Bis-Tris pH5.3, 20%(w/v) PEG3350, 0.01M KCl
Space group	P 12_11	P 3_121
Resolution	2.09 Å	2.7 Å
Misssing residues	HigA (none) HigB (101-104)	HigA (1-3, 95-104, 131-138) HigB (99-104)
No. of helices in HigA	9	7

Figure S1. **Comparison of overall structural quality of E. coli HigBA complex structures from PDB.** A, B) The graphical representation of the quality of the structure is taken from the PDB validation report for PDB 6KML (A) and PDB 5IFG (B). C) Key differences observed between two structures.

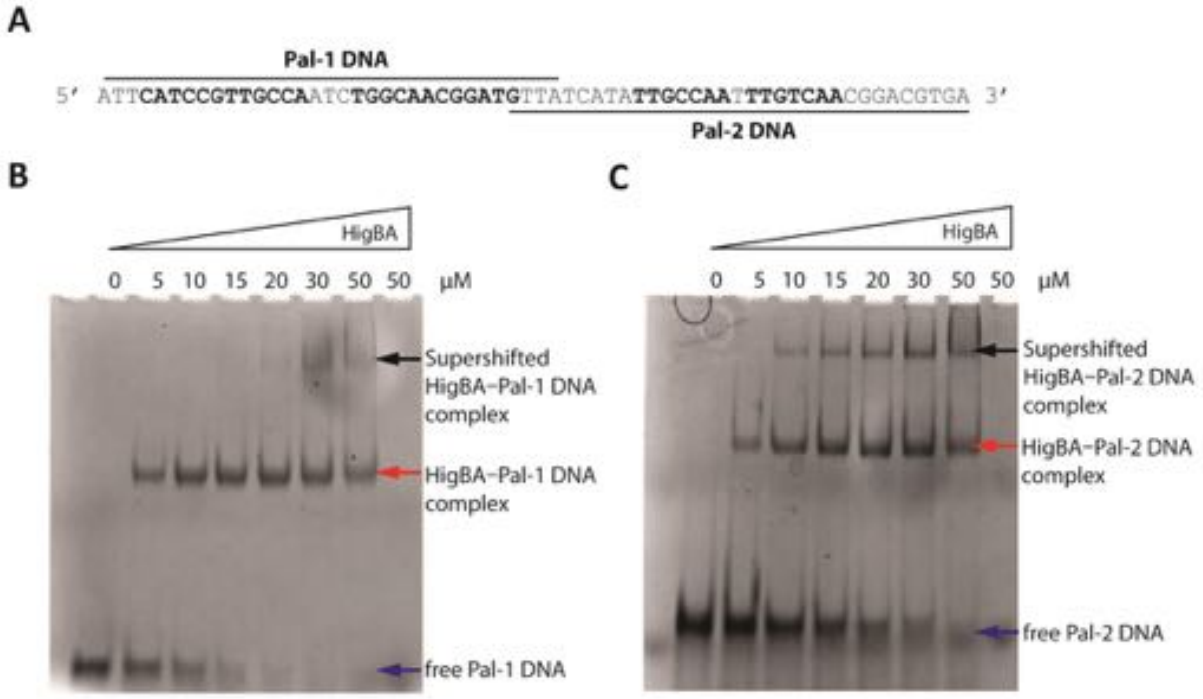

Figure S2. HigBA complex binds to the promoter DNA sequences. A) Promoter region of HigBA operon divided into two sequences designated as Pal-1 and Pal-2. The inverted repeats present in these DNA sequences are shown in bold. B) & C) Stoichiometric gel-shift assays of interaction of HigBA tetramers with Pal-1 (B) and Pal-2 (C) dsDNAs. The DNA concentration is constant (10 µM), while the concentration of HigBA complex increase from 0 to 50 µM. The last well has 50 µM only protein complex. The band corresponding to free DNA is marked with blue arrow, while the shifted and super-shifted bands are indicated with red and black arrows respectively.

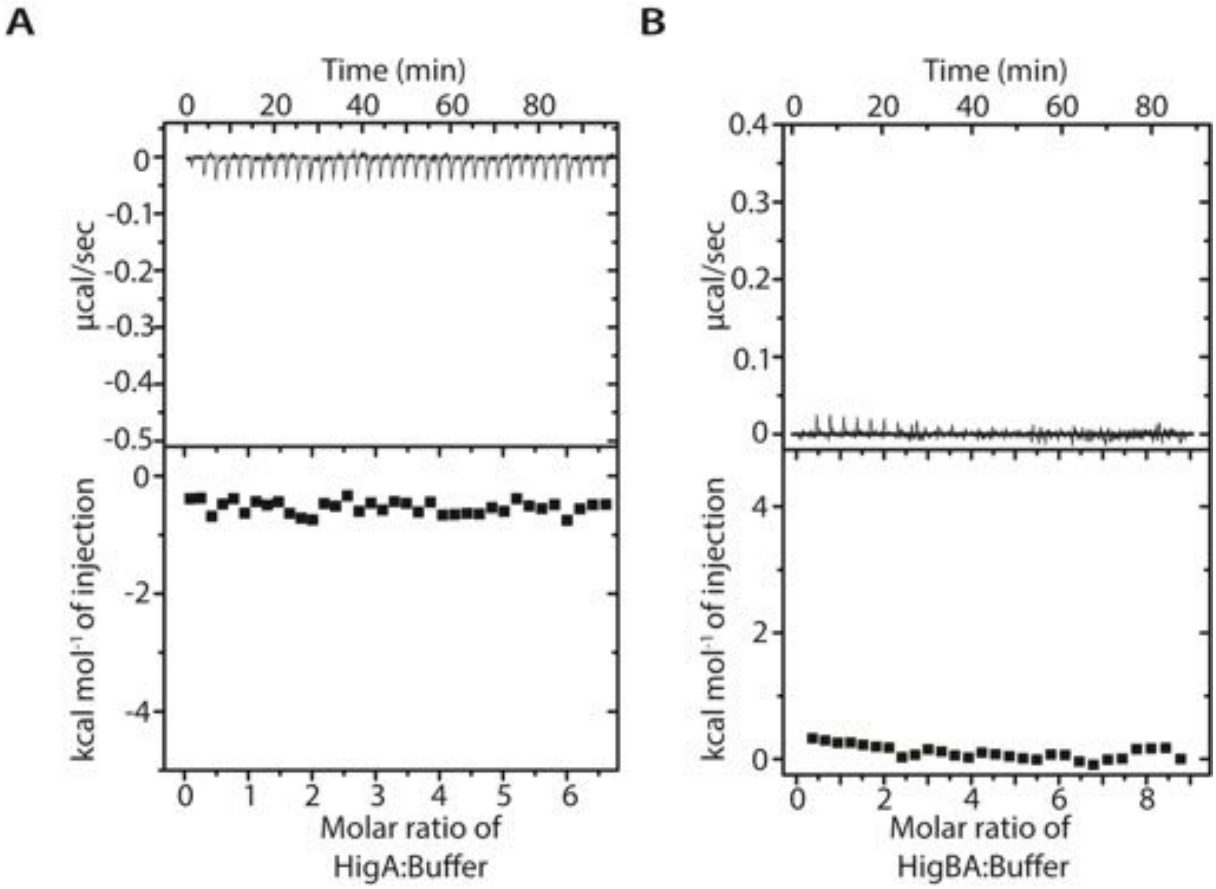

SI Figure S3. Control ITC runs of proteins titrations into buffer solution. A) ITC isotherm of HigA homodimer titrations into buffer. B) ITC isotherm of HigBA heterotetramer titrations into buffer.

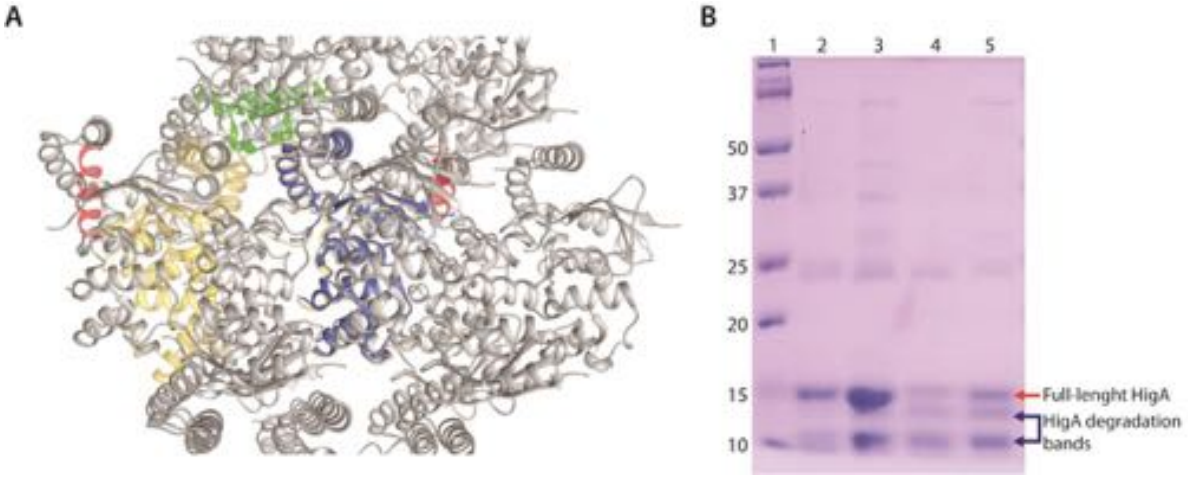

SI Figure S4: Evidence of antitoxin HigA cleavage. A) Analysis of the crystal packing in HigBA dimer (blue) vs. HigBA tetramer (straw). The HigBA dimer symmetry mates (gray) overlap with the missing N-terminal helices (green) of HigA and C-terminal helix of HigB (red). B) SDS-PAGE analysis of purified HigA protein samples show degradation. Well 1 has a protein molecular weight ladder, wells 2-5 has HigA fractions after size-exclusion column purification after incubation of 2 weeks at 4°C in a refrigerator. The red arrow marks full length HigA protein band and the degradation bands are marked by blue arrows.

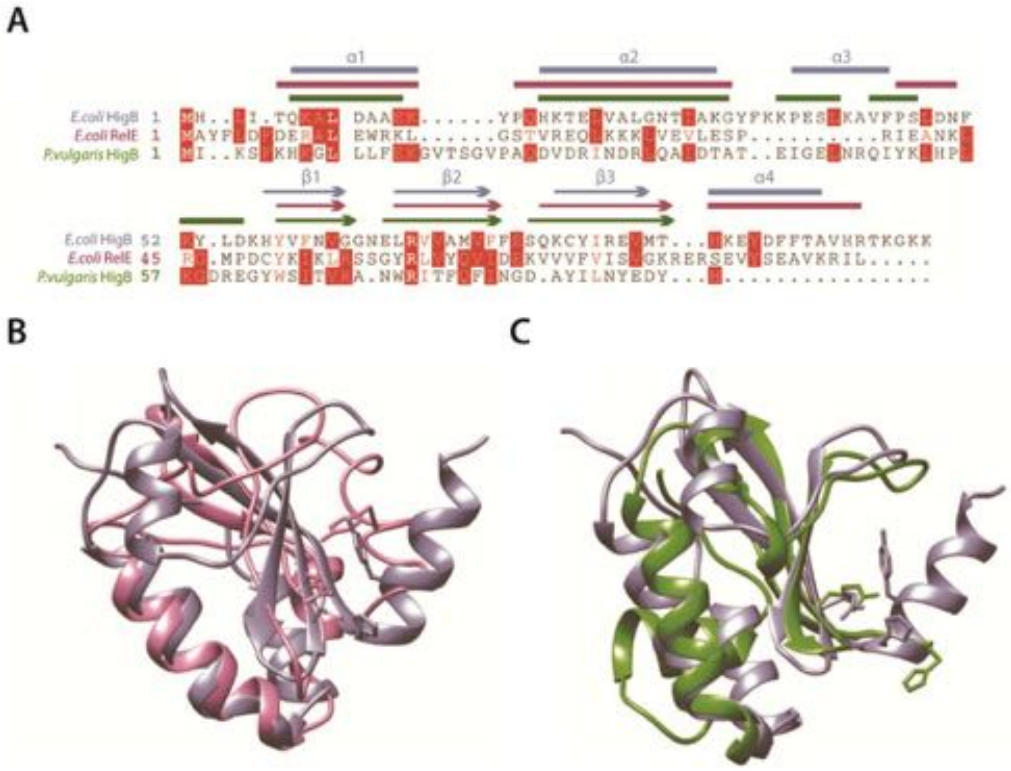

Figure S5. Sequence and Structural alignment of *E. coli* K12 HigB toxin with homologus toxins. A) Structure guided multiple sequence alignment of *E. coli* K12 HigB, E. coli RelE and P. vulgaris HigB, with secondary structure elements shown on top of the sequences. B) Overlay of *E.coli* K12 HigB (in cyan) with RelE (in purple). The conserved Arg and Tyr residues are shown in stick representation. C) Overlay of *E.coli* K12 HigB (in cyan) with P. vulgaris HigB (in green). The conserved Arg and His residues are shown in stick representation.

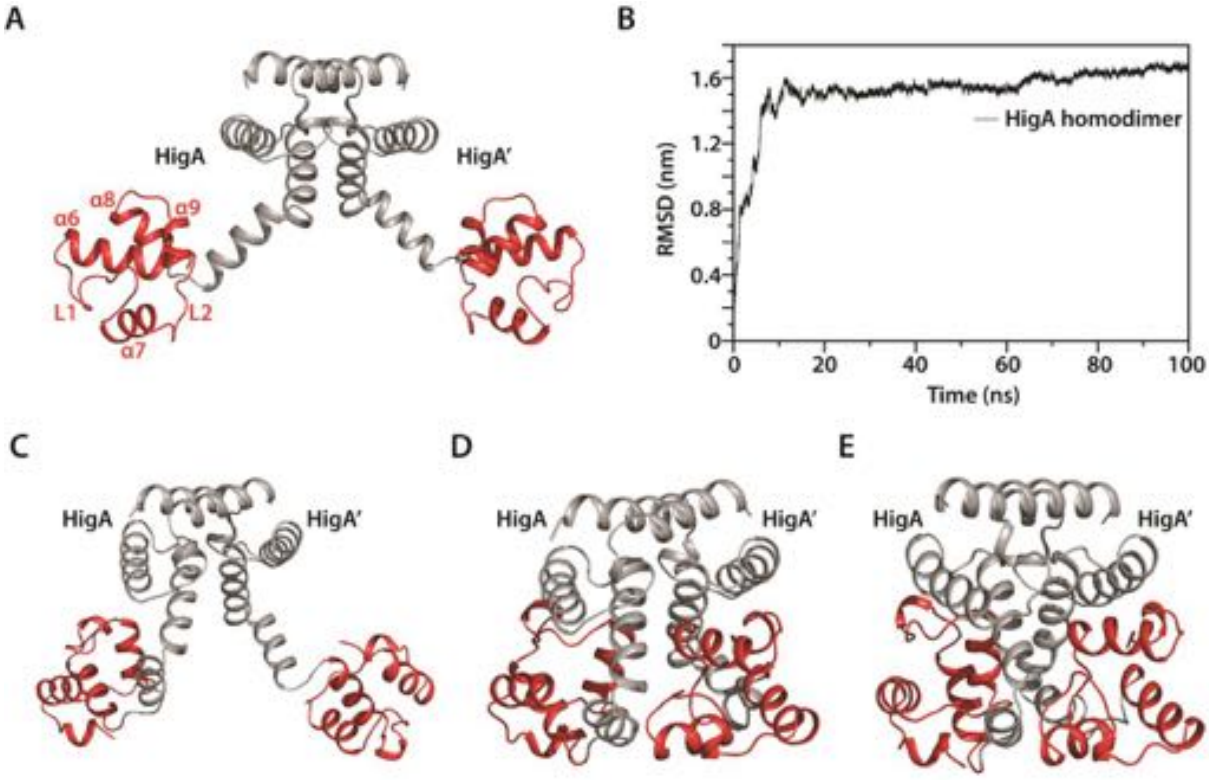

SI Figure S6: MD simulation of HigA homodimer. A) Structure of HigA homodimer, DBD is colored red and the helices in DBD are labelled for one of the protomer. B) RMSD plot of HigA homodimer for 100ns MD simulation. C), D) and E) represent structural conformation of HigA homodimer extracted from MD simulation trajectory at 5ns, 45ns and 90ns respectively.